AIMS Materials Science, 10(5): 767–818.
DOI: 10.3934/matersci.2023043
Received: 14 April 2023
Revised: 25 July 2023
Accepted: 31 July 2023
Published: 13 September 2023

http://www.aimspress.com/journal/Materials

Review

Possible magnetic performances of graphene-oxide and it's composites: A brief review

Sekhar Chandra Ray*

Department of Physics, College of Science, Engineering and Technology, University of South Africa, Private Bag X6, Florida, 1710, Science Campus, Christiaan de Wet and Pioneer Avenue, Florida Park, Johannesburg, South Africa.

*** Correspondence:** Email: Raysc@unisa.ac.za.

Abstract: Carbon-based nanostructured materials are very promising for spintronic applications due to their weak spin-orbit coupling and potentially providing a long spin lifetime. Nanostructured carbons are not magnetic materials, but intrinsic magnetic behavioral nanostructure carbon materials could be fabricated through qualitative alterations. On alterations of carbon nanostructured materials, it changes their critical temperature and magneto-crystalline anisotropy energy that could be useful as favorable magnetic materials for different magnetic/electromagnetic device-based applications. Different processes are used for the alteration of nanostructure carbon materials like chemical doping, introducing defects, changing the density of states, functionalization, intercalation, forming heterostructure and fabricating nanocomposites layered semiconductor materials. Among the carbon-based derived nanostructured materials, the graphene oxide (GO) gets attracted towards the magnet forming in the spin-like structure across the area of the magnet. Due to its magnetic behaviour, it is used for the adsorption of metals and radionuclides and to make nonconductive oxide-metal. In this review article, the basics of magnetic behavioral change of the carbon-based GO/GO-nanocomposites nanostructured materials are described by gathering information from the literature that were/are reported by different researchers/research groups worldwide.

Key words: graphene-oxide (GO); GO-nanocomposites; M-H hysteresis loop; ferromagnetic

1. Introduction

Carbon is one of the most abundant elements on earth, forming millions of chemical compounds. Among them, graphene-based carbon compounds such as graphite (few million layers of graphene) have been used in many industries, and they still hold the attention of physical and chemical engineers owing to their outstanding properties such as high specific surface area, lubricating ability, sorption, catalytic characteristics, and deaccelerating effects [1]. Graphene, the mono-layer of graphite (extracted from graphite) has been one of the most popular research topics in the past two decades because of its unique structure and properties [1–6] and has potential applications in many areas, e.g. spintronics, electronics, electrical, magnetic, catalysis, and energy storage, because of its high charge-carrier mobility and high specific surface area. In addition to these applications of grapheme, graphene oxides (GO)/reduced GO (r-GO) (also known as graphite oxide sheets) which are the derivatives of graphene are also widely used in electrochemical DNA biosensors [7,8], recyclable nano-catalysts [9], electro-analytical nano-sensors [10], electrochemical sensors [11–13], fuel cells [14] and voltametric sensors [15–18].

Graphite oxide sheets, now called graphene oxide (GO), can be made from chemical exfoliation of graphite by reactions that have been known for more than 150 years with the first instance carried out by B.C. Brodie in 1859. With oxygenated functional groups attached to its basal plane and edges, GO is insulating but can be readily dispersed in water. GO is commonly "reduced" by thermal annealing or chemical reducing agents to partially restore some of the favourable electrical, mechanical and thermal properties of the pristine graphitic sheets.

The most commonly used commercial method to synthesize large quantities of graphite-oxide, graphene-based sheets GO from graphite, is based on the Hummers and Offeman method [19]. Moreover, graphite-oxide and GO also could be synthesized by others methods *viz*. Brodie [20], Staudenmaier [21] or some modification of these methods. The dispersion of GO in water is ultrasonicated and can be readily exfoliated into single-layers called GO-sheets. The reduction methods of GO are mainly categorized into chemical reduction and thermal reduction. Typical chemical reduction of GO often requires strong reductants, such as hydrazine [22], sodium borohydride [23] and HI [24]. Other chemical reduction methods, such as photocatalyst reduction [25], electrochemical reduction [26,27] and solvothermal reduction [28], were also demonstrated for GO reduction. GO can also be directly reduced by thermal or electrochemical methods. Sometimes a combination of chemical and thermal methods is also applied for efficient reduction. The GO has a wrinkled-layered structure with greater interlayer separation than graphite. These layers are the combination of oxidized and non-oxidized regions those are randomly distributed and their relative size depends on the degree of oxidation. The oxidized regions contain mainly four oxygen functional groups *viz.* -epoxide (C–O–C), hydroxyl (–OH), carbonyl (–C=O) and carboxyl (–COOH); where the sp^2 carbon network is completely changed. It is attributed that the cutting of graphite crystal during the oxidation process, as well as the reduction process these oxygen functional groups (–OH, –O–, –COOH and C=O) breaks the π bond network on GO to create localized electronic states at their grain boundaries. In the non-oxidized regions the original sp^2 carbon network is preserved. In the oxidized regions, the epoxide and hydroxyl groups are bonded on both sides of the layer, where carbonyl (–C=O) and carboxyl (–COOH) occur at the edges of the layer. On the reduction process, the functional groups are partially removed and the sp^2 carbon network is partially restored. On reduction GO is changed into reduced graphene oxide or simply r-GO. The r-GO is not the same as

pristine graphene because a significant amount of oxygen still remains in r-GO [29]. GO is electrically insulated due to the strong disruption of the sp^2 carbon network, whereas r-GO is a low conductor compared to graphene due to the partial restoration of the sp^2 network and has the same types of defects occur as in GO. The main difference between graphite oxide and graphene-oxide is the number of layers. While Graphite oxide is a multilayer system and composed of carbon, oxygen, and hydrogen in variable ratios in a graphene-oxide dispersion a few layers flakes and monolayer flakes can be found. However, graphite-oxide and graphene oxide are chemically very similar, but structurally, they are very different. The main difference between graphite-oxide and graphene oxide is the interplanar spacing between the individual atomic layers of the compounds, caused by water intercalation.

- *Graphite-oxide*: *A compound of multilayer system and composed of carbon, oxygen, and hydrogen in variable ratios.*
- *Graphene-oxide*: *A compound of single layer or few layer system and composed of carbon, oxygen, and hydrogen in variable ratios.*

Theoretically and experimentally it is roughly known that the intrinsic magnetism can exist in graphene [30–35] and their related derivatives materials i.e. GO/r-GO. And, even covalent functionalization of GO/r-GO can induce magnetic moments [36,37]. Moreover, observing the ferromagnetism hysteresis loops of GO/r-GO, it is proved experimentally that the GO/r-GO are ferromagnetic in nature [38–44]. But the origin of the ferromagnetic behaviours are not completely conclusive due to lack of effective interactions between magnetic moments attributed mainly either to "OH"-groups [38–44] or the mixed hybridization of sp^2-sp^3 [42,43]. Interaction between randomly distributed magnetic moment in the single-layer GO structural matrix are known as surface defects that produces antiferromagnetic ordering [42,45]. These magnetic ordering are ineffective in the defected GO/r-GO/graphene-like regions due to enhancement of conduction electrons. Again, ferromagnetic ordering in zigzag graphene ribbons functionalized by an epoxy (C–O–C) pair-chain has been shown theoretically [46] that it exhibits very charming electronic and magnetic properties, and shows great promising applications in electronics and optoelectronics devices; but, the edge ferromagnetism in GO/r-GO are usually not considered because the edges of the graphite-oxide layers became functionalized in the oxidation process. Such an approach does not take into account that exfoliation results in GO flakes smaller than the original graphite layers because exfoliation methods include ultrasound irradiation that crack the GO/r-GO layers along linear defects, functionalized by epoxy groups which are often along zigzag directions [47]. However, numerous reports have suggested that oxygen-containing (carbonyl (C=O), carboxyl (–COOH), epoxy (C–O–C) etc.) and/or hydroxyl (–OH) groups are the origin of magnetism in graphene and their related materials [40,48–55]. Boukhvalov et al. suggested that the presence of hydroxyl (–OH) clusters favours magnetism in graphene and proposed that the most stable magnetic configuration in graphene sheets involves the high-spin hydroxyl groups that are formed on top of wrinkles or ripples structure [56]. Santos et al. [52] used density functional theory (DFT) to calculate the local spin moments of the carboxyl and hydroxyl groups that are adsorbed on the surface of graphene are 1.0 μB and 0.56 μB, respectively (μ_B = Bohr magneton). Wang et al. [38] also used DFT calculations to reveal that the hydroxyl group is mostly responsible for ferromagnetism in GO. It was further proposed that the presence of two hydroxyl groups bound to non-neighbouring carbon atoms that are separated by one carbon atom favours the magnetic moment of 1.0 μ_B is developed in GO. Hence, such moments developed due to hydroxyl groups are to be considered along with the moments

developed due to the defects as in graphene. If the moments are not coupled, weak para-magnetism will be observed in GO. If they are coupled by interactions, ferromagnetic, anti-ferromagnetic or super-para-magnetic behaviours will be observed in GO. However, Bagani et al. [57] presented opposing arguments for various magnetism between GO and r-GO. Bagani et al. [57] proposed that the density of wrinkles in the GO-sheets decreased upon chemical reduction at high temperature (600 ℃) owing to the removal of many epoxy groups, increasing the number of zigzag edges/edge states, causing r-GO to have greater magnetism than GO. The increase in magnetic moment is due to the increase in the number of zigzag edges/edge states after high temperature reduction (so called annealing) of GO, which are stable with the same spin to minimize the Coulomb repulsion energy. The role of oxygen-containing functional groups and hydroxyl groups in inducing magnetization in GO and r-GO sheets remains a matter of controversy and, no spatially-resolved experimental measurement to compare chemical states (or oxygen-containing and hydroxyl groups) between wrinkle and flat regions before and after chemical reduction have been conducted. Specifically, no measurement has provided any clear evidence concerning whether the high-spin hydroxyl clusters (or oxygen-containing functional groups) are truly responsible for the high magnetization on the top of wrinkles on GO-sheets, or whether the number of oxygen-containing and hydroxyl groups at the wrinkle and/or flat regions can be reduced by the reduction process. Therefore, either to enhance or to reduce the magnetic moment in GO or r-GO is not clear; so element-specific high-spatial-resolution chemical analysis is a desirable tool for directly examining the role of oxygen-containing and hydroxyl groups in particular regions, to elucidate further the difference between chemical states in specific (wrinkle or flat) regions on the surfaces of GO and r-GO sheets.

Considering all above challenges, different researchers/research groups have different opinions and have various observations that the GO/r-GO behaves like ferromagnetic or antiferromagnetic, paramagnetic and/or superparamagnetic materials. Based on these challenges, here in this work, it is reviewed, gathered most possible authentic information from the experimental observations of different researchers/research groups and hence elucidate the basics magnetic behaviours of GO/r-GO and their nanocomposites with a view on different spintronics/magnetic-based device applications. The magnetism in GO/r-GO materials is quite unique in itself as it arises from only *s* and *p* orbital electrons along with different oxygen functional groups unlike the magnetism, which arises more intuitively from the 3*d* or 4*f* electrons in traditional magnetic materials. The change in the magnetic properties have been observed as a function of sp^2-content and the presence of oxygen functional groups introduced in the structures on oxidation or reduction process. Magnetic applications of GO can no longer be considered as an emerging technology but as a rapidly expanding one. They possess a wide range of electromagnetic properties that have positioned them as serious contenders for alternative magnetic materials in the science and technology. Research in this research field, i.e. magnetic/electromagnetic applications of GO is not explored too much and their activities are limited with limited number of peer reviewed articles and conferences/workshops. This review work will provide knowledge and contributions to the emerging body of experimental and theoretical data related to magnetism and/or electromagnetism in the GO/r-GO based nanostructure materials. This review work also will be very useful for upcoming young researchers who are intend to explore the magnetic behavioural changes occurs in GO/r-GO for different most possible device based applications in science and technology community.

2. Experimental details

2.1. Preparation of graphene oxide (GO)

The GOs used in this work were synthesized mainly by the oxidation of graphite powder using a modification of Hummers' method [19] and further diluted to the required concentration using de-ionized water for further uses. In this method, 200 mg graphite powder, 100 mg sodium nitrate and ~5 mL concentrated H_2SO_4 were mixed and cooled to 0 ℃. Then the solution was kept under vigorous stirring. Afterwards, 600 mg $KMnO_4$ was added to this solution in stepwise manner so that the temperature was <20 ℃ during these $KMnO_4$ addition steps. After the complete addition of $KMnO_4$ the temperature of the solution was slowly raised to 35 ℃ and kept in this condition for 30 min. A brownish grey paste was formed. Next, ~10 mL de-ionized water was added to the whole solution and the solution turned brownish yellow. The temperature of the solution was increased to 98 ℃ during water addition and this temperature was maintained for 15 min. The whole solution was then mixed with 28 mL of warm water followed by addition of 500 μL 3% H_2O_2 that reduces the residual permanganate. The light-yellow particles were washed thoroughly with warm water 7–8 times. The solid was air dried and dissolved in ~20 mL distilled water by 15 min sonication. Then it was centrifuged at 3000 rpm for 30 min. The supernatant was collected as graphene oxide (GO) solution and used for further uses.

2.2. Preparation of r-GOs

Synthesized GO by the oxidation of graphite powder using a modification of Hummers' method [19] is diluted to the required concentration using de-ionized water for further uses. To make r-GO from GO, initially 20 mL of GO-solution with a concentration of 1 mg/mL were transferred to a Teflon-lined autoclave. The pH of the solution was adjusted to 6.5 by the addition of 0.01 M sulfuric acid. Then hydrothermal treatments were conducted at various annealing temperatures (120–180 ℃) and durations (3–24 h) for making r-GOs. The chemically modified r-GOs were washed using de-ionized water for purification. To fabricate the samples for lateral analysis, all purified r-GOs were deposited on Si substrates by drop casting at 100 ℃. In another process, synthesized GO using the modified Hummers method, moderated reduced (M-rGO) and highly reduced (H-rGO) were obtained by PT-reduction process of GO [59]. In this case, aqueous GO solutions were placed on a hot (150 ℃) Si-substrate and irradiated under a steady-state Xe lamp (500 W) for 3 and 6 h. under ambient conditions to prepare M-rGO and H-rGO [59], respectively.

2.3. Preparation of polymer coated GO (P-GO)

Different sets of 2 mL micro-centrifuge tubes were used. In one of them, 100 μL of N-(3-aminopropyl) methacrylamide hydrochloride solution (1.8 mg dissolved in 1 mL water) was inserted. In a similar way, 100 μL of polyethyleneglycol methacrylate (360 μL dissolved in 1 mL water), 100 μL of bis[2-(methacryloyloxy)-ethyl] phosphate (50 μL dissolved in 1 mL of H_2O) and 100 μL of 3-sulfopropyl methacrylate potassium salt (245 mg dissolved in 1 mL water) were inserted separately in three other micro-centrifuge tubes. Then, 0.5 mL of Igepal and 1.4 mL of cyclohexane were added to each micro-centrifuge tube and the solutions were shaken vigorously to

make them optically clear. Next, monomeric reverse micelle solutions of the four micro-centrifuge tubes were added to a three-neck flask containing 2 mL of cyclohexane. Then 500 μL of concentrated aqueous grapheme oxide solution was added to the reaction mixture and 100 μL of organic base (*N*,*N*,*N*,*N*-tetramethyl ethylenediamine) was added to the reaction mixture. The whole solution was optically clear and was kept under magnetically stirred conditions and purged with nitrogen for ~15 min to make the reaction mixture O_2 free. After that, ammonium persulfate solution (3 mg dissolved in 100 μL of H_2O) was injected to the reaction mixture as initiator. The reaction was continued for 1 h in N_2 atmosphere and then was quenched by adding a small amount of ethanol. Ethanol addition precipitates the polymer coated grapheme oxide which was washed repeatedly with $CHCl_3$ and ethanol. Next, they were dissolved in doubly distilled water. In order to remove the unbound polymer, this solution was then centrifuged at 16,000 rpm for 10 min and the precipitated particles were redispersed in fresh water. This solution was used for further applications.

2.4. Preparation of GO/r-GO and other oxide nanocomposites like r-GO:ZnO, r-GO:TiO_2; GO:MoS_2-NPs etc.

In this case, initially aqueous solution of r-GO is deposited on the Si-substrate by spin coating process and dried in open environment. After the preparation of r-GO on Si-substrate, the oxides like ZnO, TiO_2 etc. are deposited on r-GO and dried overnight. After deposition of layer by layer r-GO and metallic oxide films on Si-substrate the samples are vacuum annealed in specific temperatures depending on the nature of metallic oxide materials.

2.5. Functionalization of "Au-NP", "Fe/Fe_2O_3" and other metal and non-metal with GO/r-GO

Synthesized graphene-oxide (GO) by the modified hummer's process is subsequently reduced it with gold-nanoparticles (Au-NPs) using silica coated colloidal Au-NPs and hydrazine monohydrate solutions to form r-GO:Au-NPs nanocomposites and hence studied the magnetic properties. In case of metal/non-metal functionalization different metal/non-metal-compounds were used.

2.6. Measurements

Room-temperature/below room-temperature hysteresis characteristics M-H loop measurements were made by different researchers/research groups using either superconducting quantum interference devices (SQUID) having Quantum Design MPMS 1802 magnetometer and/or Physical Property Measurement System (PPMS), when a magnetic field was applied in the out-of-plane direction. The optical density images along with corresponding stack mapping STXM images, C *K*-edge STXM images of GO along with XANES were obtained in different beamlines from synchrotron radiation. Other measurement techniques are discussed in the respective/specific sections.

3. Results and discussion

3.1. Magnetism of graphite-oxide and heated graphite-oxide

Graphite is not a magnetic material. Each of its carbon atoms has six electrons: three of these spin pointing up while the other three point down. So, the magnetic moment of each atom is zero, making graphite diamagnetic. However, as discussed in the introduction section that graphite-oxide has a layered structure with greater interlayer separation and have two types of regions: oxidized regions and non-oxidized regions. They are randomly distributed and their relative size depends on the degree of oxidation. The oxidized regions contain four oxygen functional groups: -epoxide (–O–), hydroxyl (–OH), carbonyl (–C=O) and carboxyl (–COOH), where the sp^2 carbon network is completely changed. The epoxide and hydroxyl groups are bonded on both sides of the layer while the other occur at the edges of the layer. In the non-oxidized regions the original sp^2 carbon network is preserved. Delocalized π electrons in aromatic rings of graphite layered structures materials generally exhibit diamagnetic properties because a current along the ring produces diamagnetism when an external magnetic field is applied. But, in graphite-oxide, the π electrons develop ferromagnetism due to the unique structure of the material. The π electrons are only mobile in the graphitic regions of graphite-oxide, which are dispersed and surrounded by sp^3-hybridized carbon atoms.

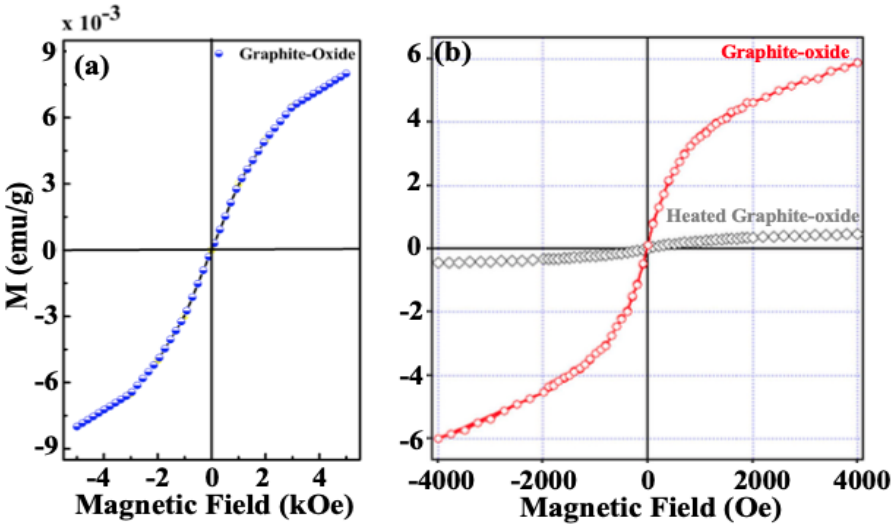

Figure 1. M-H hysteresis loops of (a) graphite-oxide and (b) graphite-oxide and heated graphite-oxide [1].

Different research groups have studied the magnetic properties of graphite-oxide. A typical M-H hysteresis loops of graphite-oxide is shown in Figure 1a that implies ferromagnetic as well as antiferromagnetic in nature. However, Lee et al. [1] have studied the magnetic properties of graphite-oxide synthesized by the Staudenmaier process [21]. Lee et al. [1] also studied in the same time the effect of change of magnetism, when graphite-oxide is heated at 250 ℃ for 24 h (known as heated graphite-oxide). Lee et al. [1] observed that the graphite-oxide is S-shaped in the M-H curve as shown in Figure 1b that exhibits ferromagnetic as well as antiferromagnetic mixed behaviours;

whereas heated graphite-oxide exhibits a linear curve in the M-H curve indicates destroyed the magnetic nature during the heat treatment (see Figure 1b). The saturation magnetization of graphite-oxide and heated graphite-oxides are 6×10^{-3} emu/g and 0.45×10^{-3} emu/g, respectively. It was discussed above that the graphite-oxide materials are composed of oxidized and non-oxidized regions. The non-oxidized regions are known as graphitic regions and these graphitic regions are damaged on thermal treatment implying more defects are produced, hence the heated graphite-oxide becomes more conductive and less magnetic in their nature [1].

3.2. Magnetism of graphene-oxide (GO) and reduced-GO (r-GO)

3.2.1. GO, Moderate (M) r-GO and Heavily (H) r-GO

As discussed above, the graphite-oxide and heated graphite-oxides are ferromagnetic as well as antiferromagnetic mixed in nature. The graphene-oxide (GO) (monolayer and/or few layer) also shows magnetic behaviour due to presence of defects and binding of O-atoms to the carbon network. The magnetic behavioural changes of GO depends on different degrees of reduction process to form r-GOs [58]. Wang et al. [59] studied and elucidated elaborately the transformation of ferromagnetic behaviours of GO into paramagnetic r-GOs on reduction. In this study, GO was synthesized using the modified Hummers method [19] and synthesized GO is reduced into r-GO by the photothermal reduction process at different levels. In the reduction process, synthesized aqueous GO solutions were placed on a hot (150 ℃) Si-substrate and irradiated under a steady-state Xe lamp of 500 W for 3 h, and 6 h respectively under ambient conditions to prepare moderate (M), and heavily (H) r-GO, respectively [59]; herein denoted as M-r-GO and H-r-GO respectively. The photo-thermal treatment changes the surface morphology as observed in field-emission SEM and TEM images shown in Figure 2a–c, and Figure 2d–f respectfully. These images show that the GO, M-rGO and H-rGO sheets are randomly stacked. In Raman spectra analysis [59], all Raman active mode *viz.* D-band, G-band, D′, 2D, (D + D′) etc. [60,61] were observed and their relative intensities ratio, say (I_D/I_G) and (I_{2D}/I_G) are changed significantly indicating the structural change occurs. The (I_D/I_G) ratios are changed from 0.91(GO) → 1.02 (M-rGO) → 0.98 (H-rGO) and (I_{2D}/I_G) ratio are changed from 0.22 (GO) → 0.15(M-rGO) → 0.32 (H-rGO), respectively. The variation of these (I_D/I_G) ratios (i.e. sp^2/sp^3 contents) is related to structural distortion, surface rippling and wrinkle-structures as also observed in SEM images (Figure 2a–c) and are formed in the graphene lattice by the restoration of C sp^2 bonds and de-oxidation upon reduction. The variations of (I_{2D}/I_G) suggested that the presence of multi-layered graphene sheets [62] in GO, M-rGO and H-rGO structure. In the PL spectra analysis [58], the width of PL lines reduced due to reduction in the number of disorder-induced defects in the π-π^* gap and the change in $sp^2 \rightarrow sp^3$ ratio upon reduction process. Figure 2g shows the normalized magnetization-hysteresis (M-H) curves of GO, M-rGO and H-rGO at room temperature after the diamagnetic contribution from the Si substrate is subtracted revealing that the ferromagnetic coercivity and saturation magnetization of GO are ~150 Oe and 3,000 Oe, respectively. The ferromagnetic behaviour of GO gradually weakens as the PT-reduction proceeds, exhibiting a paramagnetic behaviour for M-rGO and to an even greater extent for H-rGO, although the GO is typically considered to be spin-half paramagnetic [63]. The variation of M-H curves in Figure 2g, as described in the literature [40,48–55], if the ferromagnetism of the GO is dominated by the oxygen-containing and/or hydroxyl groups in the GO sheets, especially in the wrinkle regions,

then the photo thermal-reduction of GO to M-rGO and H-rGO, must have removed a rising proportion of oxygen-containing and/or hydroxyl groups from GO sheets.

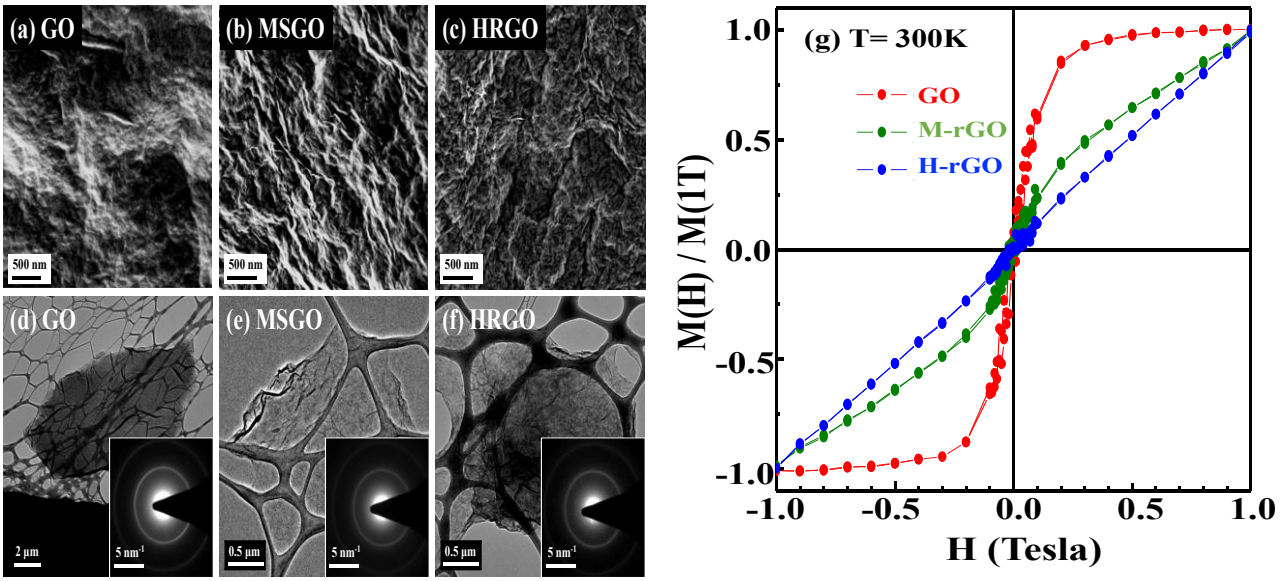

Figure 2. Field Emission Scanning Electron Microscopy images of (a) GO, (b) M-rGO and (c) H-rGO. Transmission Electron Microscopy images of (d) GO, (e) M-rGO and (f) H-rGO. (g) Room-temperature [M(H)/M(1T)]-H curves of GO, M-rGO and H-rGO after subtraction of diamagnetic background that arises from silicon substrate. Inset in Figure (g) plots M-H curves (without background subtraction) of GO, M-rGO and H-rGO [58].

Hence, the M-rGO and H-rGO sheets, with fewer oxygen-containing and/or hydroxyl groups, are paramagnetic in nature. If this argument is true, then the magnetism in GO is primarily caused by the C that is π-bonded with oxygen-containing and/or hydroxyl groups (–OH), changing the ferromagnetic behaviour of GO into the paramagnetic behaviours of M-rGO and H-rGO, as the proportion of oxygen-containing and/or hydroxyl groups varies with the degree of photothermal-reduction. To overcome this puzzle, Wang et al. [59] used X-ray microscopic and spectroscopic techniques to examine the role of oxygen-containing and hydroxyl groups in wrinkle and flat regions as well as the relationship between the C 2*p* states with defects and magnetic behaviours in GO, M-rGO and H-rGOs. For microscopic study, the optical density (OD) images of C *K*-edge Scanning Transmission X-ray Microscopy (STXM) stack mappings are shown in panel-I and panel-II in Figure 3. The decomposed STXM mappings are also shown in panels III–VI. The bright areas in the OD images represent thick regions; dim areas represent thin regions and grey areas represent the regions of intermediate thickness, as observed in GO, M-rGO and H-rGO (panel Ia–c) respectively. Based on the OD, the selected regions of GO, M-rGO and H-rGO are typically attributed to wrinkle, medium and flat regions. As presented in panels Ia–c, the brightest region of H-rGO has a higher average OD (1.29) than does GO (0.93) or M-rGO (0.64), suggesting that the thickest regions were preferably formed in the H-rGO sheets, even though they were the most heavily reduced. The various colours shown in the C *K*-edge STXM stack mapping in panels II(a–c) of Figure 3 correspond to the randomly varying thickness of GO, M-rGO and H-rGO. The

decomposed STXM stack mappings (panels III–VI) are shown in four region *viz.* blue (background), yellow (flat), red (medium) and green (wrinkle), which are directly related with various thicknesses [64] to the regions. The background is shown in blue; the OD or absorbance of the background is nearly zero, corresponding to the near-null intensity of the C *K*-edge STXM spectrum. A more intense average spectrum generally indicates a thicker region, where thickness are increasing from flat region → medium region → wrinkle region. All chemical species in these regions can affect thickness and the thick regions are typically attributed to wrinkle regions of GO sheets. Panels IV–VI in Figure 3, the flat, medium and wrinkle regions are present at random locations on the surface of GO, M-rGO and H-rGO. GO cannot be formed with a perfectly flat geometry because the wrinkle geometry of GO sheets is generally more stable than their flat geometry [65,66], so the formation of wrinkle regions of GO sheets is simply observed in both GO and r-GOs. Figure 3d,e present the C *K*-edge STXM-XANES spectra, which are the sum of the XANES spectra from the yellow, flat and green, wrinkle regions in panels IV and VI in Figure 3, respectively. The difference between the STXM-XANES spectra clarify the relationship between the chemical states that involve oxygen-containing and hydroxyl groups in flat and wrinkle regions and the magnetic behaviours of GO, M-rGO and H-rGO. The C *K*-edge STXM-XANES can be attributed to electron transitions from the C 1*s* core-level to the 2*p* final unoccupied states of GO, M-rGO and H-rGO. The magnified π* region in the insets in Figure 3d,e clearly shows the excited state of C=C (feature C_1) at ~285 eV and the wide features of C_2-C_5 in the range ~286–290 eV between the features π* and σ* of C–C, corresponding to specific oxygen-containing and hydroxyl groups in both flat and wrinkle regions of GO, M-rGO and H-rGO. These features C_2-C_5 to specific chemical states that are typically attributed to the chemical states of the C 2*p* that is bound to oxygen and hydrogen atoms [67–70]; which are specified as π*(C–OH) at ~286.4 eV, to (C–O–C) at ~287.2eV, to C=O in the –COOH bond at ~288.5 eV and to C=O at ~290.0 eV respectively [64,71,72]. However, based on the intensities of specific oxygen-containing and hydroxyl groups in both flat and wrinkle regions (higher/lower contents) of GO, M-rGO and H-rGO, if the magnetism in GO is mainly determined by the presence of oxygen-containing and/or hydroxyl groups, then the intensity of the corresponding features in the C *K*-edge STXM-XANES spectra should be significantly affected by the transformation from ferromagnetic GO to paramagnetic M-rGO and H-rGO, as seen in Figure 2g M-H curves. However, according to the insets in Figure 3d,e, after heavy-reduction, the intensities of features associated with oxygen-containing and hydroxyl groups in the wrinkle regions of H-rGO surfaces are close to those of GO, whereas those in flat regions are higher than those of GO, suggesting that the presence of the C 2*p*(*π**) states that are bound with oxygen-containing and hydroxyl groups may not be the main cause of the ferromagnetic behaviour in GO. However, the intensities of features associated with the C 2*p*(σ*)-derived states and the above features decrease with the PT-reduction of GO to M-rGO and then to H-rGO, implying the correlation between the numbers of C 2*p*(σ*)-derived states and the transformation of ferromagnetic GO into paramagnetic M-rGO and then H-rGO. This finding combined with the result that the width of the PL line-shapes is significantly reduced from GO to M-rGO and then to H-rGO, suggests that the reduction in the number of defects as reduction proceeded may importantly affect the magnetic behaviour in GO, M-rGO and H-rGO [59].

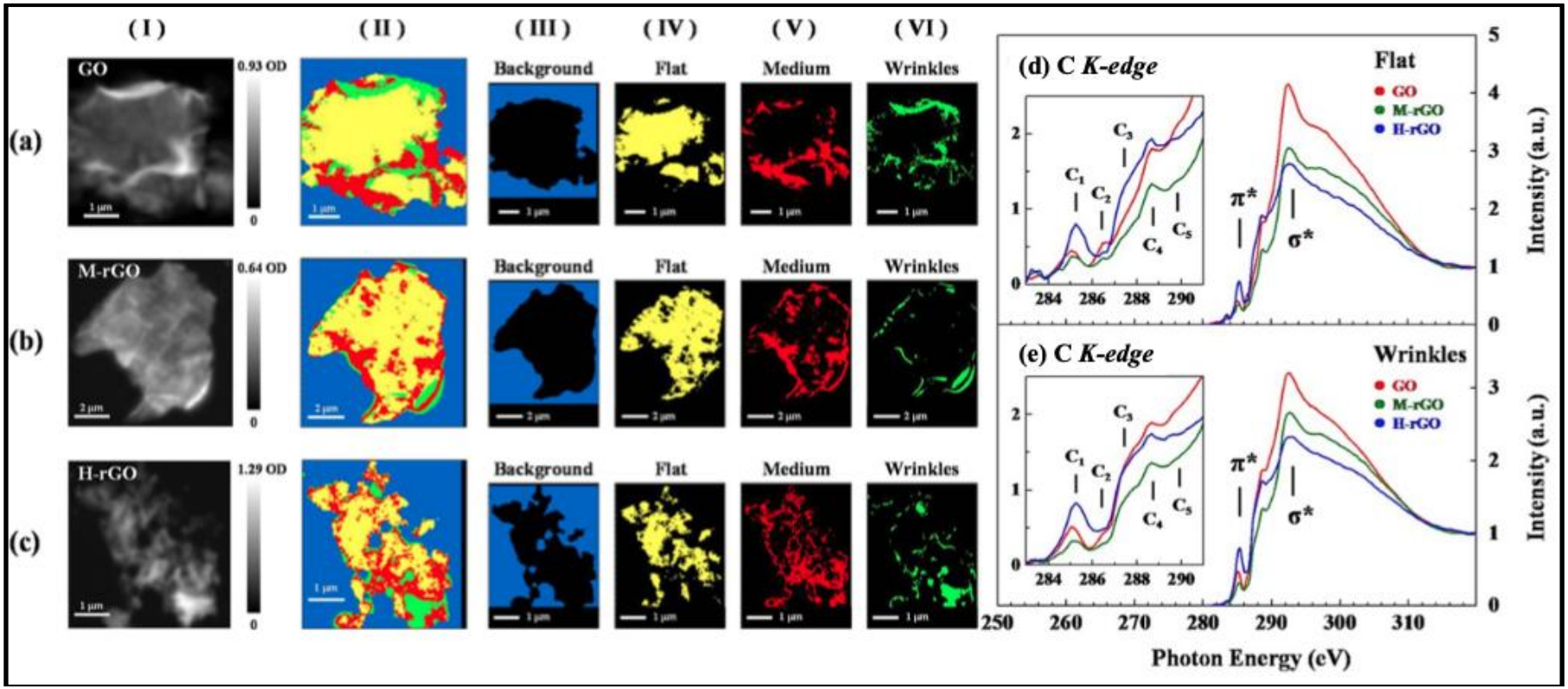

Figure 3. OD images and corresponding stack mapping from STXM images of GO, M-rGO and H-rGO are shown in panels I and II. Panels III-VI present stack mappings from C *K*-edge STXM images of GO, M-rGO and H-rGO, which are decomposed into blue, yellow, red and green regions that are associated with the different thicknesses of samples. Spectra of all samples typically present background (blue), flat (yellow), medium (red) and wrinkle (green) regions. Figure (d) and (e) presents the C *K*-edge STXM-XANES spectra of GO, M-rGO and H-rGO at flat and wrinkle regions respectively. These are the sums of XANES spectra of yellow and green regions of flat and wrinkle regions in panels IV and VI. Insets magnify 284–290 eV region of STXM-XANES spectra of flat and wrinkle regions [58].

3.2.2. Magnetism of graphene-oxide (GO) paper and GO-flakes

Strzelczyk et al. [53] studied the ferromagnetism caused at the edge of GO that become one-dimensional molecular magnets at high temperature. For this study, Strzelczyk et al. [53] synthesized GO from natural graphite using the modified Hummer's method as discussed above. Most of GOs are in suspension were monolayer. Strzelczyk et al. [53] have extracted two types of GO: (i) GO-paper and (ii) GO-flacks. GO paper was obtained by drying the GO suspension. The monolayers GO-flacks were prepared by sonication under moderate ultrasound power for 1–60 min. Magnetic M-H hysteresis loops of GO-paper were recorded at 5 K and 300 K within the magnetic field range of ±0.5 T, shown in Figure 4a. Temperature dependences of magnetization were also measured within the range of 2–300 K under zero-field cooling (ZFC) and field cooling (FC) at the magnetic field 0.03 T, as shown in Figure 4b. The M-H loops indicates that the superimposition of diamagnetic and paramagnetic components and the paramagnetic component is much weaker than the diamagnetic one.

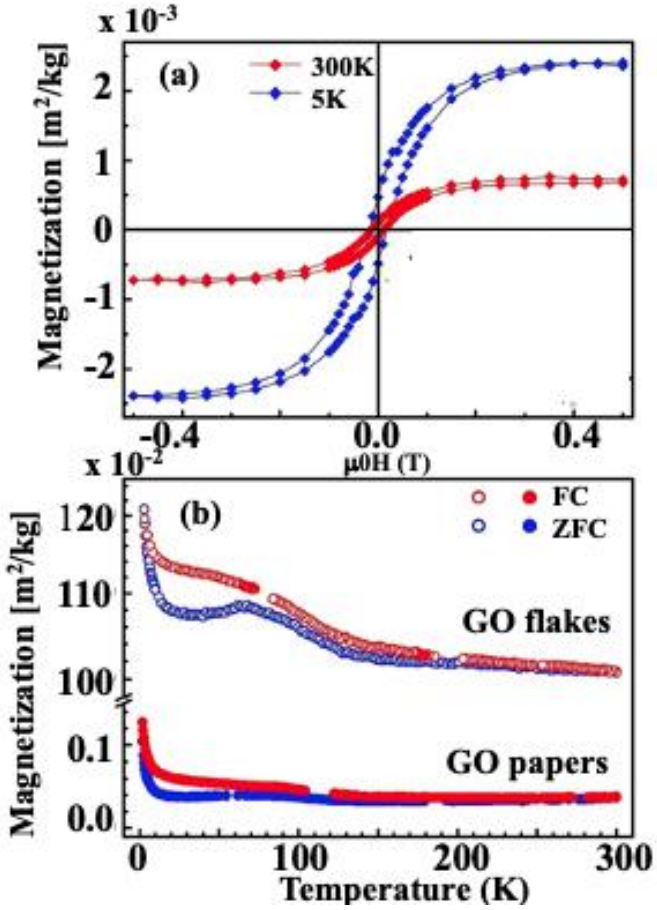

Figure 4. (a) Hysteresis loops for GO paper at 5 K and 300 K. (b) Temperature dependences of magnetization at the magnetic field 0.03 mT for GO paper and GO flakes deposited on MgO (Reproduced from Ref. [53] with permission).

The ZFC and FC curves as shown in Figure 4b show that the blocking temperatures are ≈65 K and 75 K for GO flakes and GO paper. Below the blocking temperature, thermal fluctuations

influence neither the ordered magnetic moments nor the values of the FC magnetization. However, the strong temperature dependences is observed below 20 K and cannot be explained by paramagnetic impurities as the total diamagnetic and paramagnetic contribution to magnetization estimated at 5 K and 0.03 mT is -9×10^{-4} Am^2/kg. The observed dependences suggest that the fully ordered ferromagnetic state exists below 2 K but is destroyed at higher temperatures. Regardless of the ordering process, the measured magnetization of GO flakes is 3-times higher than that of GO paper.

3.3. Magnetism of metal-functionalized graphene-oxide (GO)

3.3.1 Magnetism of "Au" functionalized graphene-oxide (GO)

Idisi et al. [73] have synthesized graphene-oxide (GO) by the modified Hummer process and subsequently reduced it with gold-nanoparticles (Au-NPs) using silica coated colloidal Au-NPs and hydrazine monohydrate solutions to form r-GO:Au-NPs nanocomposites and hence studied the magnetic properties. TEM images of typical r-GO and r-GO:Au-NPs composites materials are shown in Figure 5a,b. The TEM image of r-GO:Au-NPs composites shows that the distribution of Au-NPs on the surface of r-GO is not homogeneous. This non-uniform distribution may be due to aggregation of some particles and/or Au-NPs preferentially attached to the edge of r-GO. Details of the distribution/attachment-mechanism could be available elsewhere [74] where it is stated that the Au-NPs attachments to r-GO is due to the electrostatic interactions between r-GO and Au-NPs, and covalent-bond formation through reaction of different oxygen functional groups present on the r-GO surface on the gold nanoparticle surfaces. Idisi et al. [73] magnetic properties were studied using M-H hysteresis curve measured by a superconducting quantum interference device (SQUID)-type magnetometer. The M-H curves for the pristine r-GO and r-GO:Au-NPs were evaluated from -10 kOe < H < 10 kOe at room temperature ~300 K and at ~40 K. Figure 5c shows the measured M–H loops for the r-GO and r-GO:$(Au\text{-}NPs)_{4.88}$; with high concentration Au-functionalized r-GO:Au-NPs displaying the higher magnetization. Suda et al. [75] studied the magnetization of two different sized Au-NPs (≈1.7 nm and ≈5.0 nm in diameter) and found that the smaller particles were ferromagnetic and the larger ones were diamagnetic in nature. In this study, Au-NPs show completely diamagnetic in nature, which may be due to comparatively larger size; whereas the r-GO is ferromagnetic as also found in our earlier studies [76,77].

However, the magnetization of r-GO:Au-NPs is ferromagnetic and is higher than r-GO confirming that the ferromagnetism is enhanced on Au-functionalized r-GO. The origin of magnetisation in Au-functionalized r-GO/graphene is still controversial and not known. However, in this present case Idisi et al. [73] have found that the r-GO:$(Au\text{-}NPs)_{4.88}$ have higher graphitic in nature and even presence of higher number of oxygen functionalized groups that could be responsible for the higher magnetization. Besides the Au-NPs-content in the structures C-Au bond is also formed as observed in XPS study that induces more defects in the GO:$(Au\text{-}NPs)_{4.88}$ structure and enhanced magnetization. Figure 5d shows a linear in two cycles, within the range +1 V to −1 V. From this nature, it is clear that the conductivity decreases when Au-NPs is incorporated with r-GO. High current for r-GO can be attributed to presence of high number of sp^2-clusters. The current is reduced in r-GO:$(Au\text{-}NPs)_{0.22}$/r-GO:$(Au\text{-}NPs)_{4.88}$ composites due to reduction of sp^2-clustered by the atomic/structural re-arrangement as observed in Raman, XANES and XPS results. It is observed that

the magnetization is enhanced with reduction of electrical conductivity because the concentration of Au-NPs is higher due to formation of C–Au bonds and Au–O in the r-GO:Au-NPs nanocomposite structures. The weak attachment of Au-NPs and reduction of C–C sp^2 atoms are responsible for low mobility that leads to a drop in conductivity. As a result, the magnetization of r-GO:Au-NP nanocomposite is enhanced.

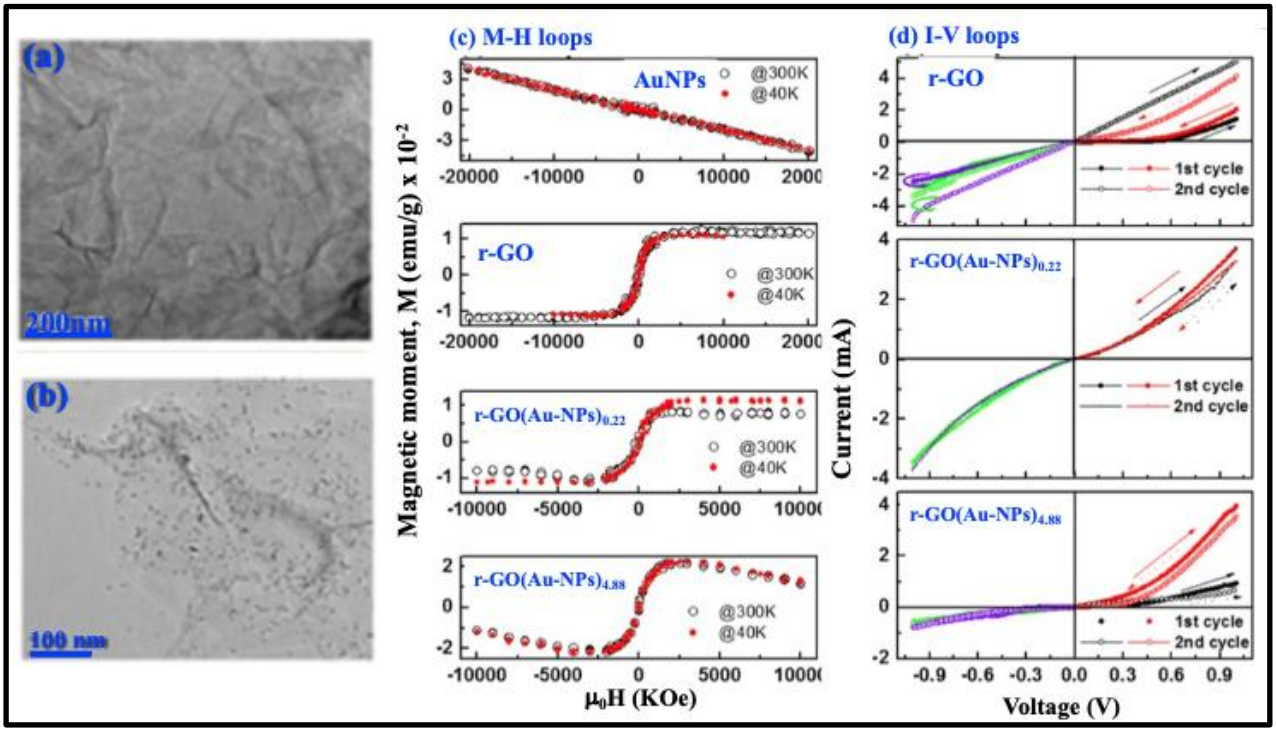

Figure 5. A typical transmission electron microscopy (TEM) image of (a) r-GO and (b) r-GO:Au-NPs nanocomposites. (c) Magnetic moment (M) versus magnetic field (H) curves of r-GO and r-GO:Au-NPs nanocomposites and (d) Current (I)-voltage (V) characteristics of r-GO and r-GO:Au-NPs nanocomposites (Reproduced from Ref. [73] with permission).

3.3.2. Magnetism of "Fe/Fe_2O_3" functionalized graphene-oxide (GO)

In the *"Fe/Fe_2O_3" functionalized graphene-oxide (GO)* structure, the TEM images of Fe-NPs and of r-GO:Fe/Fe_2O_3 nanocomposites are shown in Figure 6a,b, respectively. The morphology indicated that Fe–NPs are completely dispersed in r-GO and have formed their iron-oxide nanocomposites [78]. The images show spherical composites of the nanoscale range with an average size of Fe–NPs as ~8–10 nm. Images do not show the agglomeration of the composites but a homogeneous dispersibility of the r-GO–Fe_2O_3 nanocomposites. The formation of r-GO–Fe_2O_3 nanocomposites can be observed from Figure 6b with different particles in the composites. The current-voltage (I–V) measurements were recorded at a sweeping voltage loop of 0 to +1 V and then from +1 to −1 V and then −1 to 0. The results are presented in different ways to understand the conduction mechanism of the composites. Figure 4c,d show the linear I–V loops, and Figure 4e,f show the ln I–V loops of r-GO and r-GO:Fe/Fe_2O_3 nanocomposites, respectively. Both r-GO and

r-GO:Fe/Fe_2O_3 nanocomposites show the semiconducting behaviours with r-GO:Fe/Fe_2O_3 nanocomposites having higher conductivity. Two successive (I–V) cycle measurements show the presence of a very weak ferroelectric behaviour. The semiconducting behaviours of r-GO originate from the polarization of adsorbed molecules and the defects that might be introduced in the GO sheet during the reduction process.

The reduction in the conductivity of the first and second loops is attributed to the Coulomb blockade originating electron-hole recombination and electron tunnelling resistance. The variation in the electrical conductivity proves the importance of tuning the relationship of conductivity and relative intra-extracellular fluid volumes in tissues of MRI applications [79,80]. Idishi et al. [81] have measured the M-H hysteresis loops of GO, r-GO, and r-GO:Fe/Fe_2O_3 nanocomposites at different temperatures, *viz*., 1.8 K, 40 K, and 300 K to correlate the electrical behaviour with magnetic properties of GO as shown in Figure 6g–i. A slight dependence of magnetization on the field indicated a superparamagnetic behaviour at 300 K. It is shown that the magnetization increases with a decrease in the measurement temperature due to the atomic spins that tend to get easily aligned at low temperature [40,82,83]. GO and r-GO nanocomposites show a weak ferromagnetic behaviour, whereas the r-GO:Fe/Fe_2O_3 nanocomposite shows a superparamagnetic behaviour. The values of saturation magnetization (Ms) for r-GO:Fe/Fe_2O_3 nanocomposites is ≈0.68 × 10^{-3} emu/g (300 K) and 0.93 × 10^{-3} emu/g (1.8 K). These values are smaller than that of the bulk Fe ≈220 emu/g. The value of Ms for the nanocomposites with graphene and Fe_2O_2 contents is due to the Fe-particle size and the loading of Fe_2O_3 on the surface of graphene. Figure 6a,b reveals that the particle size of the naked Fe-loaded nanoparticles is similar indicating an inconsiderable effect of particle size on Ms, so the value of Ms depends on the loading content of Fe nanoparticles. The quantification of Fe nanoparticles was 5 at% that was estimated from XPS analysis. Super-para-magnetism makes magnetic nanoparticles disperse easily in r-GO:Fe/Fe_2O_3 nanocomposites as observed in the TEM image of Figure 4b possessing negligible magnetic interactions between each other and avoid magnetic clustering. Idishi et al. [81] have obtained the coercivity (H_C) of r-GO:Fe/Fe_2O_3 nanocomposites as ≈11 Oe and is higher than bulk Fe ≈ 0.9 Oe at room temperature (300 K) [83] comparable with superparamagnetic behaviour. The low coercivity observed in the r-GO:Fe/Fe_2O_3 nanocomposites signifies the characteristics of a soft magnet of SPIONs, which are a good candidate for MRI applications [84]. The origin of the magnetization may be attributed to the vacancies created by the hydroxyl/oxygen attached to the surface and basal plane of GO/r-GO [85]. The increase in the magnetization of r-GO:Fe/Fe_2O_3 nanocomposites with respect to GO is a consequence of defect generation due to the functionalization [86]. The defect induced from functionalization increases the crystalline size from 8 nm (GO) to 10 nm (r-GO:Fe/Fe_2O_3) and decreases Raman I_D/I_G values 0.46 (GO) → 0.43 (r-GO:Fe/Fe_2O_3). This inevitably leads to the formation of new bonds (Fe–C, C–Fe, and N=C) as indicated by XPS. Superparamagnetic behaviour has been reported previously in nanocomposites having a diameter range of 3–50 nm with a single domain magnetic particle [87]. The origin of the magnetization of r-GO:Fe/Fe_2O_3-nanocomposites may be due to the contributions of Fe–NPs atoms' presence in Fe_2O_3 because the Fe falls under 3*d* transition metals which are ferromagnetic by nature. The exchange of atoms between atoms of carbon/Fe could be the result of magnetism in r-GO:Fe/Fe_2O_3 nanocomposites. This possibility of manipulating the superparamagnetic nanoparticles of the composites by applying a magnetic field is extremely important for applications in biological and biomedical fields, particularly for magnetic resonance imaging (MRI) applications.

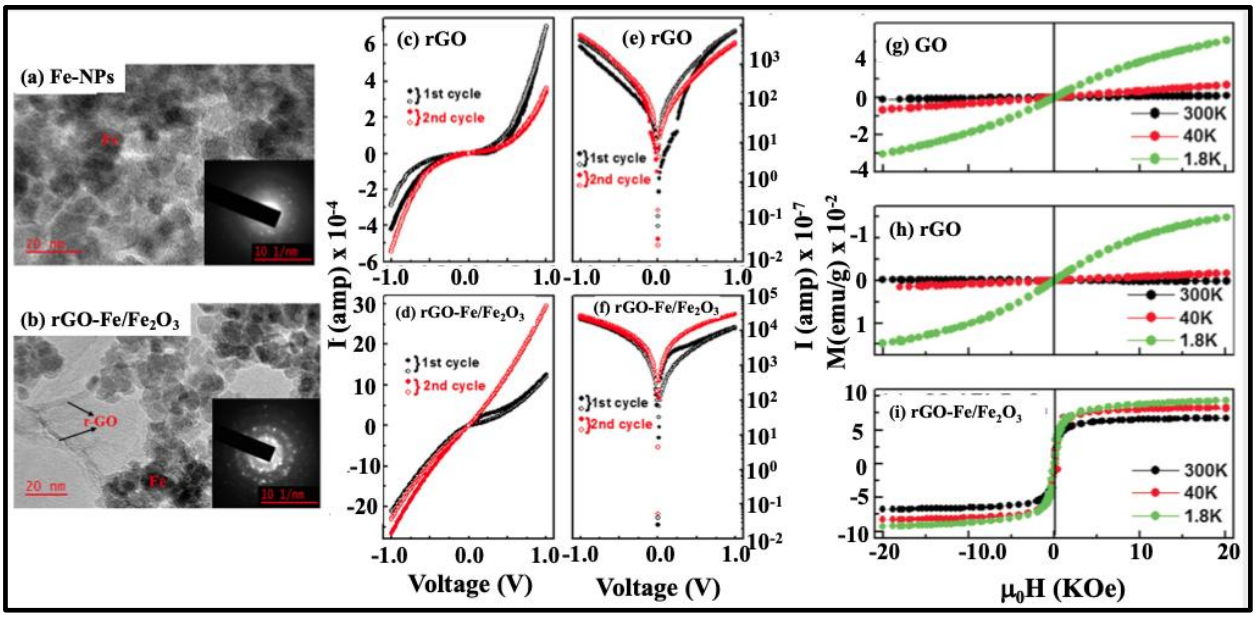

Figure 6. Transmission electron microscopy of (a) Fe-NPs and (b) r-GO:Fe/Fe_2O_3 nanocomposite. Current (I)-voltage (V) linear relationships of (c) r-GO and (d) r-GO:Fe/Fe_2O_3 nanocomposites; log(I)–(V) relationships of (e) r-GO and (f) r-GO:Fe/Fe_2O_3 nanocomposites. Magnetization vs applied magnetic field at different temperature, *viz.*, 300 K, 40 K, and 1.8 K of (g) GO, (h) r-GO, and (i) r-GO:Fe/Fe_2O_3 nanocomposites (Reproduced from Ref. [73] with permission).

3.3.3. Magnetic behaviours of r-GO:M (Bi, Pt, Ni,band Pt-Ni)-nanocomposites

Sahoo et al. [88] studied magnetic properties of r-GO along with different metal *viz.* (Pt-Ni)-, Bi-, Pt-, and Ni-nanocomposites materials. The magnetization (*M*) *vs* magnetic field (*H*) curve of r-GO, r-GO:Bi, r-GO:Pt, r-GO:Ni, and r-GO:(Pt-Ni) nanocomposites measured at 300 K are shown in Figure 7a–e; whereas zero-field-cooled (ZFC) with field-cooled (FC) magnetization of r-GO:Bi, r-GO:Ni, and r-GO:Pt-Ni nanocomposites are shown in Figure 7f–h, respectively. It is observed that the r-GO, r-GO:Ni, r-GO:Bi and r-GO:Pt-Ni nanocomposites exhibits ferromagnetism; whereas r-GO:Pt nanocomposite shows diamagnetism in nature. The ferromagnetic behaviours of r-GO come from the long-range coupling of sp^2 carbon (i.e. defects) that are formed by the removal of O-functional groups under reduction process. The Bi-metal nanocomposite *i.e.* r-GO:Bi exhibits lower ferromagnetism compared to that of r-GO because Bi-nanoparticles are diamagnetic in nature that causes a decrease in the value of magnetization of r-GO. The r-GO:Pt nanocomposite shows a diamagnetic behaviour because the elongated C–C bond conducts a much stronger coupling between the orbitals (5*d* and 6*s*) of Pt and the carbon atoms that makes diamagnetic behaviour [89,90]. In case of r-GO:Ni nanocomposite, *M-H* curve shows non-zero coercivity (H_C = 103 Oe), which is higher than bulk Ni (≈0.7 Oe) [91] and non-zero remanence (M_r = 2.3 emu/g) that confirms that the r-GO:Ni nanocomposite is highly ferromagnetic in nature.

The saturation magnetization (M_S) of 20.4 emu/g is lower than the bulk Ni metal (58.57 emu/g) [92] and is due to small crystallite grain size. This decrease in saturation magnetization in nanoparticles compared to the bulk metals is due to surface spin disorder [93] or

small size of the particles [94]. In case of r-GO:Pt-Ni nanocomposite, no M-H hysteresis loop indicates the superparamagnetic relaxation and the non-collinear moment of surface spins in the smaller particle assembly of Ni-Pt [95].

The zero-field-cooled (ZFC) and field-cooled (FC) plots of r-GO:Bi, r-GO:Ni, and r-GO:Pt-Ni nanocomposites, respectively measured at 100 Oe are shown in Figure 7f–h. All of the curves show a sharp increase in magnetization at low temperature (<25 K). This behaviour at low temperature looks characteristic of reduced graphene oxide. Such magnetic phenomenon is found when antiferromagnetic correlations compete with ferromagnetic order states. It is possible that the data correspond to a percolation type of situation, where different types of magnetic states coexist. Recent theoretical calculations indeed predict the presence of antiferromagnetic states in the sheets and ferromagnetic states at the edges of graphene [96,97]. In addition, r-GO:Ni and r-GO:Pt-Ni nanocomposites exhibit a drop also following the sharp increase. A well-defined maxima or a narrow peak around 12 K in the ZFC curve for both r-GO:Ni and r-GO:Pt-Ni nanocomposites is normally called the blocking temperature T_B [98]. There is a divergence between the FC and ZFC data in all r-GO:M nanocomposites, which is comparable to that in magnetically frustrated systems such as spin-glasses and superparamagnetic materials [96].

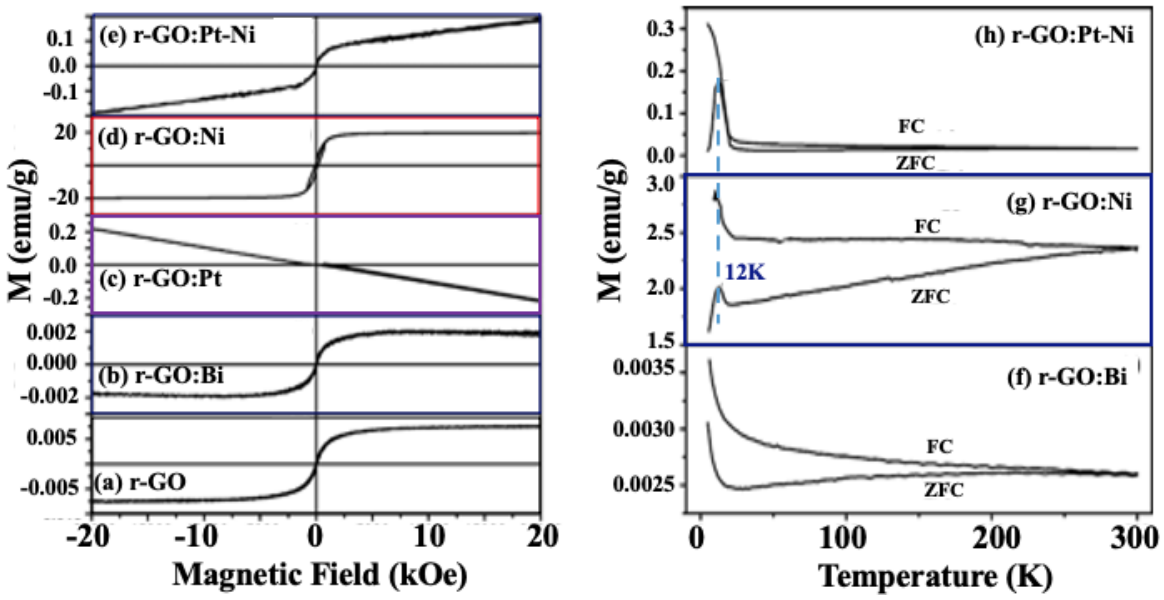

Figure 7. Magnetic hysteresis loops of (a) r-GO, (b) r-GO:Bi, (c) r-GO:Pt (d) r-GO:Ni, and (e) r-GO:Pt-Ni nanocomposites at 300 K. The ZFC and FC magnetization curves from 5 to 300 K under 100 Oe for the (f) r-GO:Bi, (g) r-GO:Ni, and (h) r-GO:Pt-Ni nanocomposites [78].

3.4. Magnetism of non-metal functionalized graphene-oxide (GO)

3.4.1. Magnetism of nitrogen-functionalized graphene oxide

Graphene oxide could be easily functionalized with nitrogen atoms. Nitrogen could also be doped with nitrogen chemically. Chemical doping/functionalization is a fascinating way to

intrinsically modify and improve the magnetic properties of graphene-oxide. Notably, among the potential dopants, the N atom is considered as an excellent candidate because it has comparable atomic size and contains five valence bonds with carbon atoms. Magnetism of graphene-oxide is of particular interest since the lightweight magnets could open up new ways to design adaptable and flexible information storage systems [99]. Especially, the greatly potential application of graphene-oxide magnets in spintronics is promising, since GO has extraordinary carrier mobility and may provide an easy way to integrate spin and molecular electronics [100]. However, GO is usually intrinsically non-magnetic and lacks of localized magnetic moments due to a delocalized π bonding network, which limits its applications in spintronic devices [101]. The point defects such as vacancies, zigzag edges and foreign atoms can induce localized magnetic moments in GO.

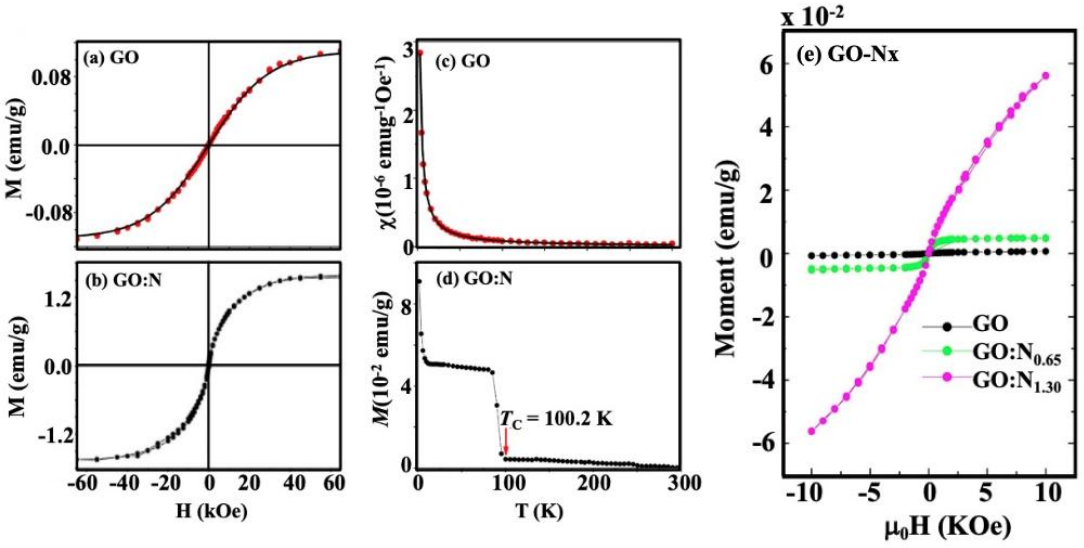

Figure 8. Typical M-H curve of (a) GO, (b) GO-N measured at ~2 K and (c,d) corresponding M-T curve [63], (e) Magnetic M-H hysteresis loops obtained for GO-Nx at room temperature (300 K) (Reproduced from Ref. [76] with permission).

Liu et al. [63] studied the magnetization increases from 0.11 emu/g (GO) to 1.66 emu/g (N-doped GO) and generated ferromagnetism with Curie temperature (T_C) of 100.2 K. For this study, N-doped graphene oxide (GO:N) was synthesized directly by annealing of GO in ammonia at 500 ℃. For GO, two factors have important influence on N content: few-layer ratio and O content of GO. Liu et al. [63] confirm that oxygen groups in GO favour the reactions with NH_3 and C–N bond formation, and directly annealing GO in ammonia can obtain high content of GO:N, which are responsible for the magnetic behaviour of GO-N. Figure 8a,b shows the typical magnetization (M–H) hysteresis curve of GO and N-GO measured at ~2 K, and corresponding M-T curves are shown in Figure 8c,d. The highest coercive field (Hc) and remnant magnetization (Mr) of 160 Oe and 0.039 emu/g, respectively are obtained from the M-H curve shown in Figure 8a, the solid evidence for ferromagnetism. The M–T measurement shows that the GO is paramagnetic in nature, whereas GO-N shows ferromagnetism and Curie temperature T_C ~100.2 K (see Figure 8c) that indicate that the Tc is above the liquid N_2 temperature of ~77 K. Sarma et al. [76] studied the change of magnetic properties of Hummer's method synthesized graphene oxide (GO), when different N_X (at%) is

functionalised with graphene oxide (GO-Nx). In this study, the M–H curves for the pristine GO and nitrogen functionalized GO:Nx were measured at room temperatures (300 K) at magnetic field (H) ±10 kOe. Figure 8e shows the measured M-H loops for the GO:$N_{1.30}$ displaying the strongest ferromagnetic behaviour with a saturation magnetization (M_s) ≈ 5.3 × 10^{-3} emu/g and a coercivity (H_c) of ≈10 Oe. On the other hand, the magnetic saturation of GO:$N_{0.65}$ is M_s ≈ 4.9 × 10^{-4} emu/g and the coercivity (H_c) ≈ 19 Oe, higher than that of pristine GO having M_s = 6.8 × 10^{-5} emu/g with coercivity (H_c) ~38 Oe. The origins of magnetisation in N-doped GO/graphene are still controversial wherein ferromagnetism in N-doped GO has been ascribed to pyrrolic groups which can provide a net magnetic moment of 0.95 μ_B/N atom [102–105]. In contrast, Ito et al. [104] have observed that the presence of pyrrolic groups lead to a reduction in the magnetisation values. Sarma et al. [76] have found in this study that the GO:$N_{1.30}$ have higher graphitic in nature and is responsible for the higher magnetization. Besides the N-content, GO:$N_{1.30}$ become more disordered, i.e. enhancement of sp^2-content in the GO structure and hence magnetization is enhanced. The magnetisation in sp^2 carbon structures also originate from defects as well. Moreover, the valence band photoemission spectra of GO/GO-Nx [76] shows that the electronic density of states (DOS) of GO-Nx is significantly higher than the GO as a result of the magnetic properties also enhanced on GO-Nx. In another report, Ghosh et al. [77] studied the magnetic behavioural change of nitrogen functionalized graphene oxide (GO-Nx) using four different nitrogen (N) precursors *viz.* ammonium hydroxide (NH_4OH), hexamethylenetetramine ($C_6H_{12}N_4$), acetonitrile (C_2H_3N), and carbamide (CH_4N_2O) and found that the $C_6H_{12}N_4$ based-*GO-*N_x shows higher magnetic behaviour. Ghosh et al. [77] further functionalized the $C_6H_{12}N_4$ based-*GO-*N_x with iron oxide using three different iron (Fe) precursors *viz.* ferric oxide (Fe_2O_3), ferrous oxide (Fe_3O_4), and iron oxide-hydroxide (FeOOH) to tune this room temperature ferromagnetism (RTFM). Iron can be present in graphene oxide composites in the elemental form or as Fe-core/oxide shell nanoparticles, iron oxides and among others. The ratio of iron nanoforms in different oxidation states depends, in particular on O-containing groups (-Epoxide (C–O–C), Hydroxyl (–OH), Carbonyl (–C=O) and Carboxyl (–COOH)) present in the GO-surface, use of reductants, and other conditions. These iron-containing nanoparticles are loaded on the GO and their growth mechanism. XRD, SEM and TEM measurements shows the structural and surface morphological study as shown in Figure 9a–d, whereas Magnetic M-H hysteresis curves are shown in Figure 9e–f. XRD results show that the synthesized $C_6H_{12}N_4$ based "*GO-*N_x" and Fe_2O_3-based "*GO-*N_x*:Fe*" composites, respectively are the characteristic peak corresponding to the reflection from the C (002) plane in the graphitic structures. The increase in the full width at half maximum (FWHM) of the peak of C (002) plane in the Fe_2O_3-based "*GO-*N_x*:Fe*" indicates the nominal disorder induced by Fe-particles. The C (002) diffraction peak also shifted that related to the change in the stress caused by imperfections within the "*GO-*N_x*:Fe*" lattice, such as interstitials and stacking faults. A few peaks marked by "Δ" is coming from the "Fe" and/or oxides of "Fe" present in the "*GO-*N_x" structure. Figure 9b shows the field emission scanning electron microscopy (FE-SEM) image of the $C_6H_{12}N_4$ based "*GO-*N_x". Figure 9c,d shows the TEM images of synthesized $C_6H_{12}N_4$ based "*GO-*N_x" and Fe_2O_3-based "*GO-*N_x*:Fe*", respectively. Comparing the TEM images of "*GO-*N_x" and "*GO-*N_x*:Fe*" confirms the formation of composite materials with the characteristic of two dimensional (2D) layer structure of graphene-oxides. Images also show that the "*GO-*N_x*:Fe*" decreases the contrast of individual "*GO-*N_x" structure and covered with Fe-particles. The measured magnetic M-H hysteresis curve within the magnetic field range −10,000 Oe < H < +10,000 Oe at room temperatures (300 K) of those four types of "*GO-*N_x" that are shown in Figure 9e.

The magnetization of "*GO-N*$_x$" does not only depend on the content of carbon and/or nitrogen, but also strongly depends on different N-precursor. Figure 9f shows that the highest magnetization was obtained in "*GO-N*$_x$" synthesized with $C_6H_{12}N_4$-precursor, with the saturation magnetization (*M*s) value of 0.0057 emu/g and a coercivity (*H*c) of 53 Oe; whereas the lowest magnetization was found (*M*s = 0.0031 emu/g and *H*c = 31 Oe) in "*GO-N*$_x$" synthesized with CH_4N_2O-precursor. This magnetic behaviour also depends on the formation of different N-functional groups, like pyridine-N, pyrrolic-N, graphitic-N and N-oxide, different carbon-carbon bond and carbon-oxygen functional groups such as –OH, –COOH, C–O/C=O that are attached with the "*GO-N*$_x$" matrix during the formation of "*GO-N*$_x$" [106]. However, the origin of this magnetization in N-doped GO is still controversial [107,108]. There are some reports on ferromagnetism in N-doped GO that has been ascribed due to pyrrolic-N group which can provide a net magnetic moment of ≈0.95 μ_B/N atom [103]. In contrast, Ito et al. have observed that the presence of a pyrrolic group leads to a reduction in the net magnetization value of nitrogenated GO [104].

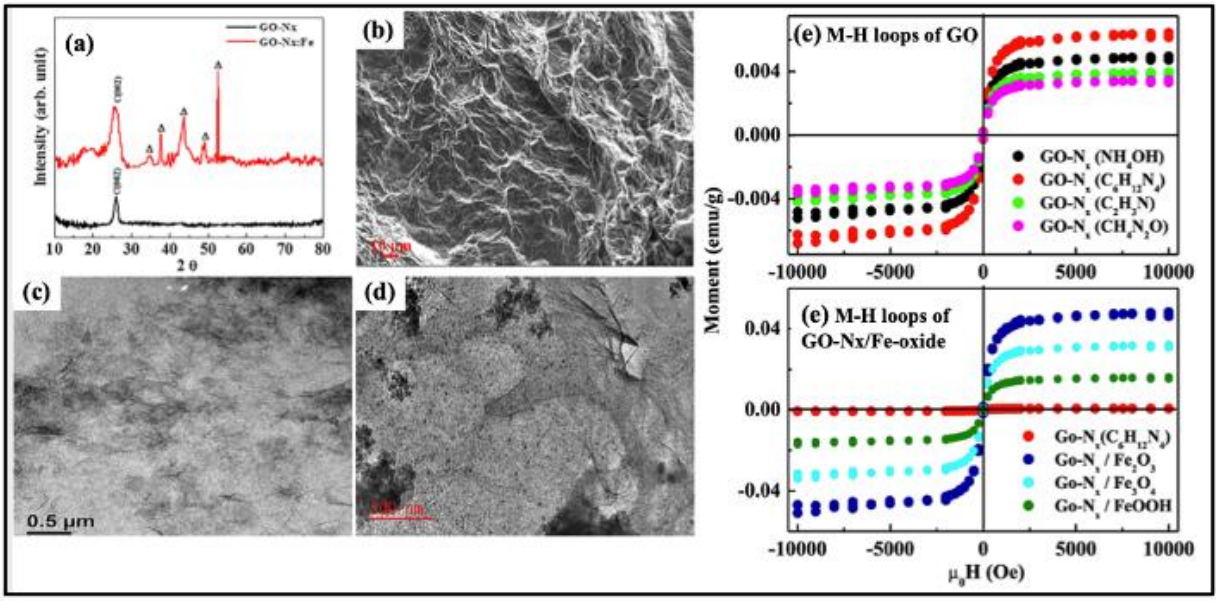

Figure 9. (a) XRD of synthesized $C_6H_{12}N_4$ based "*GO-N*$_x$" and Fe_2O_3-based "*GO-N*$_x$*:Fe*" respectively (∆ are "Fe" and/or oxides of "Fe"); (b) FE-SEM image of as synthesized $C_6H_{12}N_4$ based "*GO-N*$_x$"; (c) TEM image of as synthesized $C_6H_{12}N_4$ based "*GO-N*$_x$" and (d) TEM image of as synthesized Fe_2O_3-based "*GO-N*$_x$*:Fe*". Magnetization M-H loops of (e) NH_4OH-based "*GO-N*$_x$", $C_6H_{12}N_4$-based "*GO-N*$_x$", C_2H_3N-based "*GO-N*$_x$" and CH_4N_2O-based "*GO-N*$_x$"; (f) Magnetization M-H loops of Fe_2O_3-based "*GO-N*$_x$*:Fe*" composites, FeOOH-based "*GO-N*$_x$*:Fe*" composites and Fe_3O_4-based "*GO-N*$_x$*:Fe*" composites (Reproduced from Ref. [77] with permission).

3.5. Magnetism of polymer-functionalized graphene-oxide (GO)

Ganya et al. [109] studied the magnetism of pure polymer-functionalized GO and established a correlation with electrical behaviour of these materials. In this study, utilizing a reverse micelle process, Ganya et al. [109] have grafted polyacrylate (P) on graphene oxide (GO) to realize

polyacrylate grafted graphene oxide (P-GO) nanocomposites and hence upon subsequent reduction, polyacrylate grafted reduced graphene oxide (P-rGO) nanocomposites were achieved and studied the electrical and magnetic behaviour. For the electrical measurements, the linear current-voltage (I–V) relationship for GO/r-GO/P-rGO were obtained (Figure 10a,c,e) by sweeping the voltage in the sequence $0 \rightarrow +1 \rightarrow 0 \rightarrow -1 \rightarrow 0$ V using a step voltage of 0.01 V. As expected, GO showed poor conductivity and highly insulating behavior owing to the heavy oxidation of the carbon lattice. With the subsequent removal of oxygen functional groups and an increase in the sp^2 content of the films (as confirmed by XANES and Raman spectroscopy), the r-GO films showed a significantly enhanced (~10^6 times higher) current response. The grafting of polyacrylate, a nonconducting polymer, onto GO (P-GO) leads to lower (~10^4 times than r-GO) current response owing to the extended polymer chains hindering the charge flow as well as the higher sp^3 content. However, P-rGO current response is nearly ~10^2 higher than that of GO, albeit still lower than r-GO, which can be attributed to the lower amount of oxygen functional groups [81,110]. The corresponding log I–V curves for GO/r-GO/P-rGO are shown in Figure 10b,d,f in which the GO shows a symmetric log I–V curve, which has a small hysteresis loop on the positive voltage side and ranges between 0 V and 0.5 V, while P-rGO displayed a small hysteresis loop on the positive voltage side in the range 0.25–0.75 V. The hysteresis effects usually arise from deeply trapped charges due to the presence of defects in P-GO as the escape time for the trapped charges is longer than the time it takes to make the semi-log sweep [111]. Ganya et al. [109] observed that the sheet resistances of GO, r-GO, and P-rGO are 4×10^9 Ω/sq, 2.5×10^3 Ω/sq, and 3.3×10^7 Ω/sq, respectively, that are comparable with the reported values [112].

The measured magnetic behaviour via M-H hysteresis loops at 2 K and M-T characteristics curve at 500 Oe are shown in Figure 10g,h. A weak paramagnetic behaviour was observed for GO with a saturation magnetization (M_S) $\approx 4.6 \times 10^{-3}$ emu/g and $\approx 5.6 \times 10^{-3}$ emu/g for r-GO with low coercive field values (H_C). For both GO and r-GO, the observed magnetic behaviour arises due to the contributions of defects and the nonbonding π-electron states localized at the graphene layer edges, i.e., dangling bonds at the edge planes, as corroborated by XANES measurements [86,113,114]. For both cases, a variety of defects including topological defects, vacancies, adatoms, wrinkles, corrugations, etc., besides the binding of oxygen atoms to the carbon lattice can give rise to magnetic moments [86,113,114]. In the case of GO, the hydroxyl group bonded to C-atom of the sublattice too can induce a local magnetic moment. In fact, Wang et al. [52] have shown that a magnetic moment of 1.2 μ_B is developed in the case when a hexagonal graphene ring is bonded to two hydroxyl groups. Such a magnetic moment developed due to oxygen moieties should be considered along with the defect induced magnetic moment for the total magnetic behaviour of GO. Extensive literature reports suggest that not only the de-oxygenation itself but also its underlying process, i.e., hydrazine [63], thermal [57], or Birch [115] reduction, strongly influence the magnetic properties of the resulting r-GO. However, Ganya et al. [109] used a strong reducing agent like hydrazine hydrate that introduces significant defects as well as N-dopants into the r-GO graphitic lattice that generates a localized magnetic moment [63]. It has been argued earlier as well that as compared to GO reduced in a hydrogen environment, the use of ammonia (nitrogen) conditions leads to the oxygen concentration being more efficiently reduced with simultaneous introduction of N-defects leading to higher magnetization [116]. It has also been shown by Taniguchi et al. [117] that localized electronic states in r-GO also add spin moments to the sp^2 nanodomains, which result in singly occupied molecular orbital levels in the π-π* gap leading to the emergence of magnetism. For both GO and

r-GO, an increase in the magnetization with the reduction of temperature was observed owing to the ease of the alignment of magnetic spins at low temperatures ~2 K. However, for both GO and r-GO, as the magnetic moments are not coupled, only weak para-magnetism is observed ($M_S \approx 4.6\times10^{-3}$ and $\approx5.6 \times 10^{-3}$ emu/g for GO and r-GO, respectively). However, had the magnetic moments been coupled by long-range interactions, ferromagnetic, antiferromagnetic, or superparamagnetic behaviour should have been observed. The measured values of GOs are similar to those reported by Qin et al. [116]. The grafting of diamagnetic polyacrylate on its own is not expected to enhance the magnetic response of the composites, and indeed the maximum magnetization of the P-GO ($M_S \approx5.5 \times 10^{-3}$ emu/g) is very similar to that of r-GO. However, upon reduction of P-GO into P-rGO, a near doubling of the M_S value to $\approx9.6 \times 10^{-3}$ emu/g was observed. Furthermore, considering P-rGO, the saturation magnetic moment was found to be $\approx2.79 \times 10^{-3}$ emu/g with a remanent magnetization value of $\approx8.6 \times 10^{-6}$ with a coercivity value of nearly ≈12 Oe. As mentioned earlier, despite their suitable applications in bioimaging, the lack of magnetic moment renders pristine GO is not suitable for MRI applications. However, the possibility of improving its magnetic response by introducing defects or manipulating oxygen functionalities renders it an excellent candidate for MRI contrast agents [118]. Enayati et al. [118] reported on the variation of the magnetic properties of GO produced by strong and weak oxidizing agents, which were then further exposed to 1.23 MeV γ-rays. It was observed that as compared to weak-GO (Ms ≈ 0.013 emu/g), strong-GO showed higher magnetization (Ms ≈ 0.023 emu/g), which was further expressed upon its reduction ($M_S \approx 0.033$ emu/g) [118]. Furthering their work, the irradiated samples were further annealed at various temperatures (200–800 ℃) to enhance their magnetism. It was observed that at 600 ℃, the saturation magnetization not only reached a maximum value of nearly 0.16 emu/g but the r-GO samples showed no toxicity when measured using an MTT [(3(4-(4,5-dimethylthiazol-2-yl)−2,5-diphenyl-tetrazolium bromide)] assay and as such has been proposed as an alternative MRI contrast agent [118,119]. Considering the GOs prepared in this work, as the GO itself is nonstoichiometric, consequently the resulting P-rGO system too is chemically quite complex, where it includes a variety of oxygen and nitrogen surface moieties and topological, adatoms, and structural defects, all of which can contribute to the magnetic moment. In terms of the defects, it has been previously reported by He et al. [120] that the magnetization of HOPG is closely correlated to the defect density with an almost linear relationship observed between the I_D/I_G ratio (i.e disorder and graphitic) and magnetization. Indeed, P-rGO shows the highest defect density value. Considering this along with the quantification from the XPS analysis, P-rGO shows the highest nitrogen content (~1.9 at%), and as such, the highest magnetization is expected arising due to the extra π-electron from nitrogen making the structure electron-rich, thereby enhancing the magnetic coupling between magnetic moments [63,121,122].

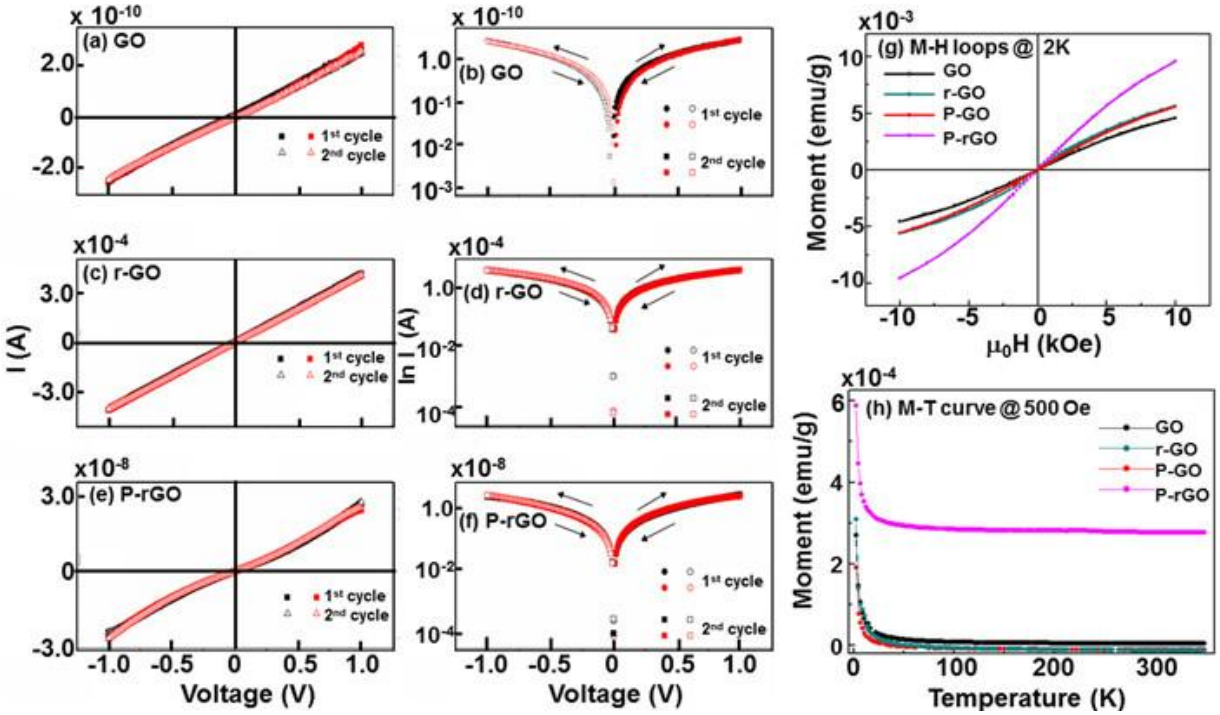

Figure 10. Linear current (I)-voltage (V) relationship for (a) GO, (c) r-GO, and (e) P-rGO samples with the corresponding log (I)-(V) relationship shown in (b), (d), and (f) respectively. (g) Magnetization (M) vs applied magnetic field (H) loops obtained at a temperature of 2 K and (h) magnetization (M) vs temperature (T) curve obtained at an applied field of 500 Oe (Reproduced from Ref. [109] with permission).

However, there is still debate in terms of the effect of the various nitrogen functional groups, especially the pyrrolic and pyridinic nitrogen moieties, and how they affect the magnetization of graphene. Ito et al. [104] have observed that the presence of pyrrolic groups lead to a reduction in the magnetization. Miao et al. [103] have observed enhanced ferromagnetism in N-doped graphene with high pyrrolic content, which was shown to include a net magnetic moment of 0.95 $_B$/N-atom. Theoretical calculations also reveal that graphitic N does not contribute to the magnetism in graphene and in the case where there are paired defects, such as graphitic-graphitic, graphitic-pyrrolic, and graphitic-pyridinic N pairs, the system prefers a nonmagnetic state [123]. Simultaneously, it was shown that pyrrolic nitrogen in the carbon lattice becomes more stable when the defect site is bonded to hydroxyl or carbonyl groups [123]. From Raman and XPS measurement, it was observed that a small amount of pyrrolic nitrogen was only observed in the case of P-GO and P-rGO, which had a higher defect ratio and amount of carbonyl groups. Density functional theory calculations have shown that when pyridinic nitrogen is bonded to oxygen, then the system becomes spin-polarized [62] with a magnetic moment of ≈0.56 μB. Considering that P-rGO still contains a considerable amount of oxygen (20 at%), there is a high possibility that the pyridinic nitrogen can interact with some of the oxygen groups either in the r-GO lattice or indeed in the polyacrylate itself or that the magnetic behaviour is more expressed due to the parallel spin orientation between the nitrogen and oxygen radicals, especially at low temperatures [124]. Thus, the enhanced magnetization in P-rGO can be ascribed to high defect density, N-doping, and enhanced magnetic coupling between the magnetic moments. Ganya et al. [109] believed that the possibility of

manipulation of this magnetic behaviour along with the abundance of surface functional groups makes both P-GO and P-rGO highly conducive for deriving water-soluble functionalized graphene by linking affinity molecules with polyarylate backbone for future biological and biomedical applications. Ganyn et al. [125] also studied the magnetism of conducting polymer functionalized graphene oxide. In that work, Ganyn et al. [125] synthesized GO/r-GO by the same conventional Hummer's method [19] and functionalized with PEDOT-PSS (CP-rGO) composites. This method of preparing the composites was used due to its simplicity, cost effectiveness, and also to avoid agglomeration of nanoparticles [126]. The scanning electron microscopy (SEM) micrographs of GO, rGO, and CP-rGO composite structures are shown in Figure 11a–c, respectively. The GO exhibits multi-layered flaky structures which are aggregated, reflecting the multi-layered microstructure. GO sheets are not well connected, crumpled, and have a high surface area with smooth morphology. This observation indicates adequate exfoliation of graphite during the chemical oxidation process. The r-GO micrographs consist of flaky structures, scale-like layered structures that are evenly distributed and overlapping to form a compact structure. This observation exhibits the restoration of the graphene plane as the oxygen-related functional groups are removed due to the reduction process of GO to r-GO [127]. CP-rGO exhibits flaky structures that are not as overlapping as in rGO and the flakes have a large surface area. CP-rGO also presents a porous 3D network structure with a few folds indicating rGO nanosheets being homogeneously coated by PEDOT-PSS to form sandwich-like structures.

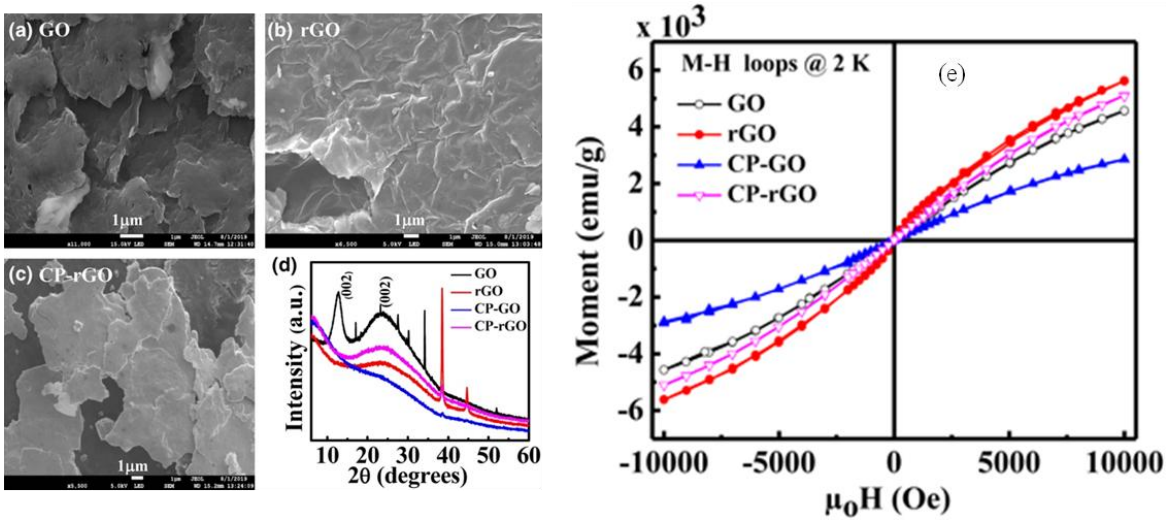

Figure 11. SEM images of (a) as-synthesized graphene oxide (GO), (b) reduced graphene oxide (rGO), and (c) conducting-polymer coated graphene oxide (CP-rGO). (d) XRD patterns for GO, rGO, CP-GO, and CP-rGO. (e) Magnetization (M) versus applied magnetic field (H) loops obtained at a temperature of 2 K of GO, r-GO, CP-GO, and CP-rGO (Reproduced from Ref. [125] with permission).

The XRD patterns for GO, rGO, CP-GO, and CP-rGO nanocomposites are shown in Figure 11d. A sharp C (002) peak was observed at ~12.7 ºwith a full width at half maxima (FWHM) of ~2.19 º. This peak corresponds to an interlayer *d*-spacing of 0.697 nm. The increased *d*-spacing in GO with respect to graphite results from the formation of oxygen-containing functional groups between

graphene layers making them thicker and possibly intercalation of water molecules trapped between adjacent GO sheets [128,129]. In contrast to GO, r-GO displayed a broad C (002) peak at ~24.3 º (*d*-spacing = 0.366 nm) with a high FWHM of ~9.14 º, indicating the presence of defects/ strains [129,130]. The r-GO exhibits a pristine graphite structure considering its smaller *d*-spacing value resulting from the formation of very thin r-GO layers when GO is reduced with hydrazine hydrate [128]. Broad peaks were observed at 23.6 º(*d*-spacing ≈ 0.377 nm) with an FWHM of ≈8.97 º and ≈23.9 º(*d*-spacing ≈ 0.371 nm) with an FWHM of ≈10.27 ºfor CP-GO and CP-rGO, respectively. The slightly higher *d*-spacing values for CP-GO and CP-rGO can be attributed to the presence of oxygen-containing functional groups and the formation of defects and PEDOT-PSS coating on the GO/rGO sheets by polymers [109]. In GO, the main contributor to its magnetism is the magnetic moment developed due to the presence of oxygen moieties like the hydroxyl group bonded to the C-atom of the sublattice [52]. As for r-GO, its magnetic properties are strongly influenced by the reduction process, of which in our case, the strong hydrazine hydrate reducing agent introduces significant defects through attaching nitrogen dopants onto the r-GO graphitic lattice thereby generating a localized magnetic moment [116]. Considering that r-GO had pyridinic-N bond only and these bonds lead to an increase in the defect structures, this resulted in r-GO recording a maximum Ms value [86,131]. It was observed that the magnetization of GO and r-GO increases with decrease in temperature at 2 K, due to the ease in alignment of magnetic spins at low temperature. Notably, the measured Ms values for GO and r-GO are of the same order (but show better magnetization) as those reported by Idisi et al. [81]. Singh et al. [132] studied the GO/r-GO-coating PEDOT-PSS materials and observed the lowering of highly magnetic materials, and as expected, CP-GO recorded a low Ms value of ≈2.9 × 10^{-3} emu/g, whereas CP-rGO had a relatively high Ms value of ≈5.1 × 10^{-3} emu/g. Considering that CP-GO had a very low I_D/I_G ratio as compared to GO, this implied that CP-GO had a lower defect density; hence, less magnetic behaviour as expected is observed. On the same note, CP-GO had a lower defect density as compared to rGO, thus resulting in a relatively lower saturation magnetization than rGO. Regardless of the low defect density in CP-rGO in comparison to GO, a higher saturation magnetization was observed in CP-rGO as a result of high nitrogen content (~3.2 at%) leading to enhanced magnetic coupling between magnetic moments [121,133]. Importantly, the observed weak para-magnetism observed in all our samples results from magnetic moments not being coupled by long-range interactions; otherwise, ferromagnetic, anti-ferromagnetic, or super-paramagnetic behaviour should have been observed. In addition, the electrical measurements show that the sheet resistance of GO, rGO, CP-GO, and CP-rGO are ~4.0 × 10^9, ~2500, ~1.0 × 10^5, and ~9.0 × 10^5 Ω/square, respectively. The sheet resistance of rGO decreased upon reduction as compared to that of GO due to the removal of oxygen functional groups and a subsequent increase in the sp^2 content (as verified by XANES and Raman spectroscopy). Also, the PEDOT-PSS-coated GO recorded a lower sheet resistance as compared to the starting GO due to incorporation of PEDOT-PSS a conducting polymer. The rGO with a work function of ~4.0 eV had the lowest sheet resistance, whereas the PEDOT-PSS-coated nanocomposites with relatively lower work functions had sheet resistance of the order 10^5 Ω/square. Elk et al. [134] reported on lower conductivity as a result of higher density of states, which is in agreement with our results where PEDOT-PSS-coated nanocomposites indicate an increase of DOS at/near VBM or E_F and resulted in higher sheet resistance as compared to rGO. These electrical properties are the most suitable properties for electrical and electrochemical biosensor applications. The measured magnetic behaviour through M-H hysteresis loops from −10 to +10 kOe at ~2 K

curves is shown Figure 11e, Paramagnetic behaviour was displayed by GO and r-GO with a saturation magnetization (Ms) of ≈4.5 $\times 10^{-3}$ and ≈5.6 $\times 10^{-3}$ emu/g, respectively. As for rGO at 2 K, it had a remanent magnetization value of ≈6.2 $\times 10^{-6}$ emu/g and a low coercive field value (H_C) of about 5 Oe. The observed magnetic behaviour for both GO and rGO emanates from lattice defects and nonbonding π-electron states localized at the graphene layer edges, i.e., dangling bonds at the edge planes, as evidenced by our XANES measurements [131]. The defects observed in GO and rGO are mainly vacancies/voids, zig-zag edges, adatoms, wrinkles, corrugations, etc. [86,121,131].

3.6. *Magnetic properties of GO/r-GO-nanocomposites*

3.6.1. Magnetic behaviour of Fe_3O_4:r-GO nanocomposites

See et al. [135] studied the magnetic behaviour of the magnetically separable r-GO/Fe_3O_4 nanocomposites. In this work, different weight ratios of GO and Fe_3O_4 were used for the preparation of rGO:Fe_3O_4 composites materials and vibrating sample magnetometer (VSM) was used to carried out the M-H loops at room temperature (300 K) for both the bare Fe_3O_4-nanoparticles and the r-GO: Fe_3O_4 nanocomposites, and the results are shown in Figure 12. The bare Fe_3O_4 nanoparticles and the r-GO/Fe_3O_4 nanocomposites showed typical *S*-like curve magnetization hysteresis loops with no coercivity, inferring that they exhibit super-para-magnetism, while their magnetization behaviours were removed in the absence of the applied magnetic field. The saturation magnetization (Ms) of the r-GO:Fe_3O_4 nanocomposites increased from 1.63 emu/g to 30.30 emu/g with an increase in the content of Fe_3O_4 nanoparticles in the r-GO sheets. The saturated magnetization value observed for the pristine Fe_3O_4 nanoparticles was 58.70 emu/g, which was higher than that of the magnetic r-GO/Fe_3O_4 nanocomposites. This can be attributed to the presence of graphene in the nanocomposites [136].

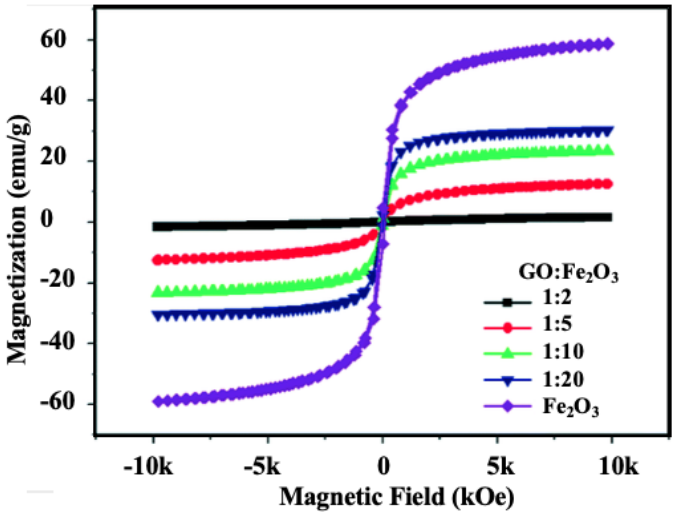

Figure 12. Magnetization M-H curves of GO:Fe_2O_3 (1:2), GO:Fe_2O_3 (1:5), GO:Fe_2O_3 (1:10), GO:Fe_2O_3 (1:20) and Fe_2O_3 [135].

Tanwar et al. [137] studied the magnetic behaviours using the magnetic material, magnetite

(iron oxide) with GO and rGO nanocomposites within the applied magnetic field ≈−5 kOe to +5 kOe. In this study, Tanwar et al. [137] found that the GO and r-GO are diamagnetic behaviour [138] at room temperature which gets converted into superparamagnetic behaviour upon magnetite doping as confirmed by *S*-like curves of magnetic hysteresis loops that both nanocomposites behaves super-para-magnetism at the room temperature. Incorporation of magnetite-nanoparticles in the GO/r-GO affect the stability of nanocomposites in the presence of an external magnetic field shows magnetic response of the nanocomposites. Saturation magnetizations are 3.45 emu/g and 3.92 emu/g for magnetite (iron oxide)-GO and magnetite-rGO nanocomposites respectively and are smaller than the reported value of bulk Fe_3O_4 of 92 emu/g [139] due to the relatively low amount of magnetite loaded on GO/r-GO. Thapa et al. [140] engineered the magnetic GO in the nanocomposite form of iron oxide nanoparticles-graphene oxide (GO) and studied the magnetic behaviours. These nanocomposite of magnetic iron oxide (magnetite) nanoparticles with GO/r-GO have a large number of applications in various fields such as drug delivery [141], imaging [142], batteries [143,144], catalysis and environmental remediation [145].

3.6.2 Magnetic performance of r-GO thin film deposited on "ZnO-NR:ncAu

Ray et al. [146] studied ferromagnetic performances of r-GO composites with ZnO-NR:ncAu. In this study, the M-H hysteresis loops are measured at/below room temperature (~300 K/2 K), which are shown in Figure 13a–d, whereas Figure 13e–h shows M-T during field cooling (FC) and zero-field cooling (ZFC) at the applied magnetic field of 2500 Oe. Comparing the earlier reported results about the ferromagnetic behavior of pure ZnO-NR and *nc*-Au/ZnO-NRs [147], it is confirmed that the corresponding ferromagnetism performance of ZnO-NR:r-GO and (*nc*-Au/ZnO-NRs):r-GO is significantly enhanced. For a comparable study, we have obtained different magnetic parameters, *viz*., the saturation magnetization (Ms), and coercivity (Hc) values from the M-H hysteresis curve. It was believed that the magnetic performances are enhanced in (*nc*-Au/ZnO-NRs):r-GO composites due to the formation/interaction between magnetic *nc*-Au and O vacancies and/or zinc vacancy (*V* Zn) or zinc interstitial (Zn*i*) present at the interface of (*nc*-Au/ZnO-NRs):r-GO [147]. It is attributed to the cut of the r-GO crystal during the oxidation/reduction process of various oxygen functional groups (–OH, –O–, –COOH, and C=O) that break the π bond network at grain boundaries [1,148–151], inducing the magnetic domain. The r-GO sheets have unsaturated π orbitals (*p*z) and a lack of bandgap. This is favourable for the electronic interaction with 3*d* orbitals of transition-metal ions in oxide semiconductors and, hence, enhances the magnetizations. It is also energetically favourable to place the epoxy groups on the opposite side of hexagonal rings that induce a magnetic moment. At the same time, a high concentration of sp^3 type defects (OH) remained on the basal plane of r-GO sheets, which effectively induced magnetic moments.

Figure 13e–h show the dependence of magnetic susceptibility on temperature for a nanocomposite ZnO-NRs/rGO in ZFC and FC modes at an applied magnetic field H = 2500 Oe. There is no significant difference in magnetic susceptibility in ZnO-NRs:r-GO, and (*nc*-Au/ZnO-NRs-10):r-GO is due to the presence of parallel magnetic moments, whereas in (*nc*-Au/ZnO-NRs-15):r-GO and (*nc*-Au/ZnO- NRs-30):r-GO, there is a significant difference in their magnetic susceptibility due to the possibility of setting some anti-parallel magnetic moments. It is observed that two transitions of magnetic moment at ≈250 and ≈35 K exist in these composite systems, which may be mainly due to two composites, ZnO-NRs with *nc*-Au and r-GO, respectively.

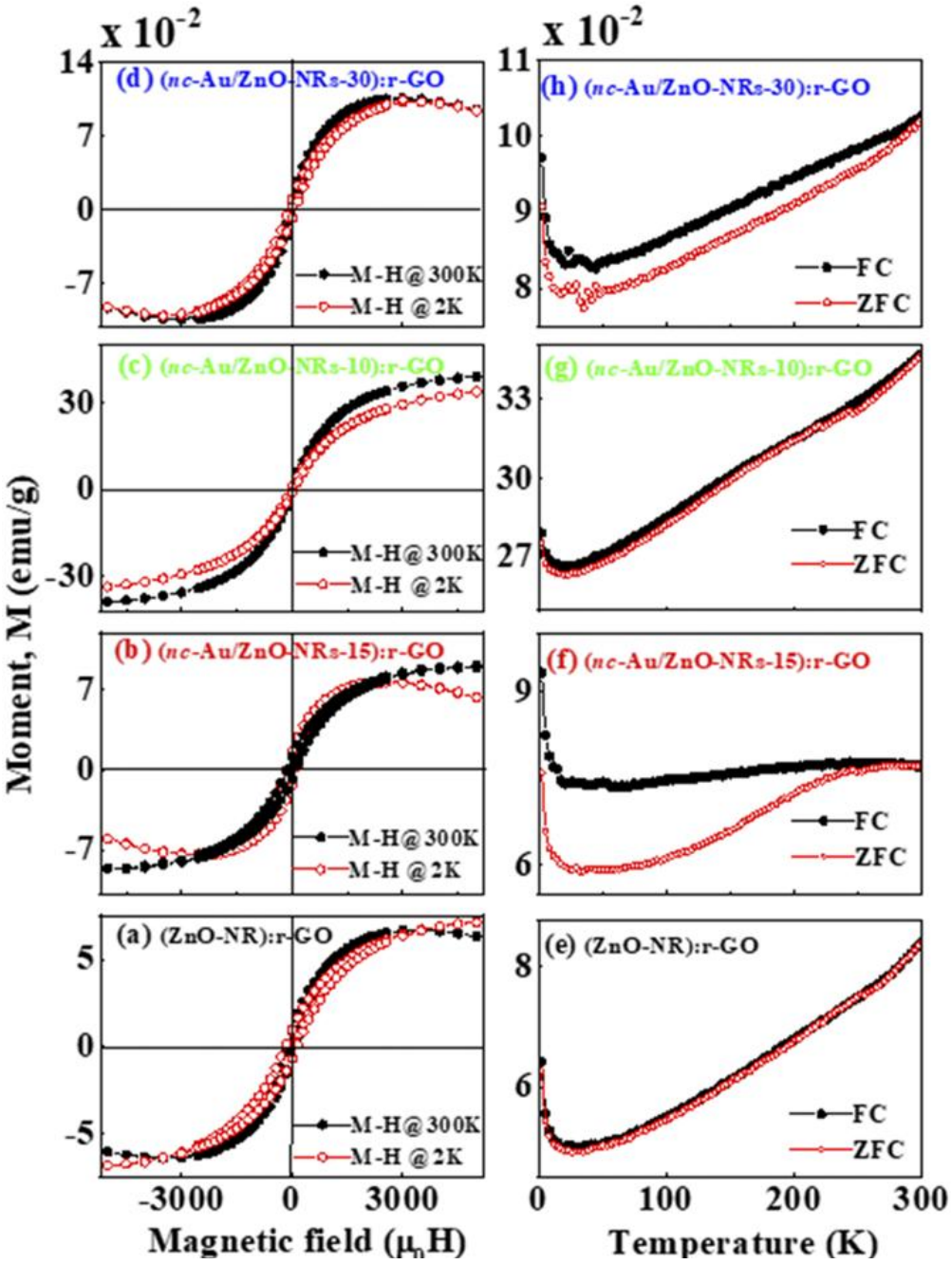

Figure 13. M-H hysteresis loop of (a) ZnO-NR:r-GO, (b) *nc*-Au/ZnO-NRs:r-GO (Au-4-10-15), (c) *nc*-Au/ZnO-NRs:r-GO (Au-4-30-10), and (d) *nc*-Au/ZnO-NRs:r-GO (Au-3-10-30). The M-T curve of (e) ZnO-NR:r-GO, (f) *nc*-Au/ZnO-NRs:r-GO (Au-4-10-15), (g) *nc*-Au/ZnO-NRs:r-GO (Au-4-30-10), and (h) *nc*-Au/ZnO-NRs:r-GO (Au-3-10-30) [146].

3.6.3. Ferromagnetism in rGO-ZnO nanocomposites of (r-GO:ZnO)

Thiyagarajan et al. [152] studied interfacial ferromagnetism in reduced graphene oxide-ZnO nanocomposites (r-GO:ZnO). In this study, GO was synthesized using modified Hummer's method and then different forms of GO:ZnO-nanocomposite (labelled as SrGO–ZnO, 1HrGO-ZnO, and

2HrGO-ZnO nanocomposites, respectively) were prepared using Zinc acetate dehydrate [$Zn(CH_3COO)_2 \cdot 2H_2O$] [152] at different conditions. The magnetization M-H hysteresis curves of GO, rGO SrGO–ZnO, 1HrGO-ZnO, and 2HrGO-ZnO nanocomposites were measured at room temperature within applied magnetic field ≈ -15 kOe $< H <$ 15 kOe are shown in Figure 14. They found that GO is weak ferromagnetic with dominant diamagnetic signals. As discussed above, the GO is composed of an unreacted graphite (sp^2) region and a reacted (sp^3) region with partially distorted layers with randomly distributed epoxy, hydroxyl, carbonyl and carboxyl functional groups on each plane. Carboxyl and carbonyl groups are located at the edge sites of GO sheets, whereas hydroxyl and epoxy groups are adsorbed on the basal plane of GO sheets. The epoxy groups on the opposite side of hexagonal ring induce a magnetic moment. The graphitic edge state is magnetically active due to the presence of non-bonding with a large local density of states that are populated with unpaired electron spin to minimize the coulomb repulsive energy, leading to large moments at the zigzag edge boundary. At the same time, high concentration of sp^3 type defects (OH) on the basal plane effectively induced magnetic moments.

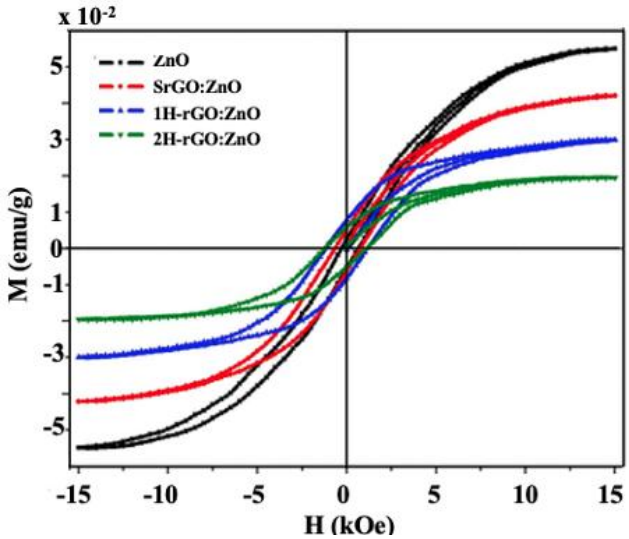

Figure 14. M–H hysteresis curve of the ZnO, Sr-GO:ZnO, 1H-rGO:ZnO and 2H-rGO:ZnO nanocomposites. [Hydrothermally reduced 160 mg of GO dispersed (1 mg/1 mL) product was named as 1HrGO and 320 mg of GO dispersed (2 mg/1 mL) product was named as 2HrGO (Reproduced from Ref. [152] with permission).

In this present study, weak ferromagnetism arises due to interaction between separated magnetic regions and domains. The diamagnetic contributions are due to the attachment of carbonyl and hydroxyl groups located at edge site and on the basal plane of GO, respectively. On reduction of GO sheets, remove the functional groups that causes defects in the form of vacancies, structural defects and distortion in the lattice of GO, which leads to ferromagnetic behaviour at the zigzag edges in 1H-rGO/2H-rGO. At the same time, some of the damaged sp^2 carbon conjugations were restored and generated partial coalescing of r-GO sheets that increases the amount of π–π staking sites, which increase the density of defects as a result increase spin moment in r-GO sheets. Removal of carbonyl groups can compensate the dangling bond and preserve the edge states magnetism. Reduced wrinkles contain local magnetic anisotropy energy density and coming out of longer range magnetic

interaction/ordering that long range ordering (magnetically coupling) of these spin exists due to a tiny crystalline size and a large quantity of grain boundaries among small portions of rGO sheets, which contributes to the ferromagnetism. Room temperature M-H hysteresis loops of ZnO and rGO:ZnO nanocomposites are shown in Figure 14, where ZnO and rGO:ZnO nanocomposites clearly exhibits ferromagnetism. The origin of ferromagnetism in ZnO-nanostructures is associated with various kinds of structural defects *viz.* oxygen vacancies, zinc vacancies, zinc interstitials and oxygen interstitials present in the lattice sites that induces magnetic moments. The population of defects in ZnO is usually not large and uniform, and the magnetization value of these specimens is very small compared to magnetic oxides. The high surface to volume ratio of ZnO has a higher density of oxygen vacancies and creates surface spin disorder. These uncontrolled formation of lattice defects during preparation processes, forms the isolated spin magnetic moments in lattice site of ZnO.

3.6.4. Magnetic performance of r-GO thin film deposited on TiO_2 (TiO_2:r-GO)

Ray et al. studied the magnetic performances of a TiO_2:r-GO nanocomposite [153]. Figure 15a shows the magnetization vs applied magnetic field (*M-H*) hysteresis loops of r-GO, TiO_2, and r-GO/TiO_2 that are measured at room temperature (~300 K) and below the room temperature (~40 K), whereas the *M-T* curve during FC and zero-field cooling (ZFC) are shown in Figure 15b–d. From the *M-H* hysteresis loops and the *M-T* curve during field cooling (FC) and ZFC, it is very clear that magnetization is enhanced when r-GO is deposited on the TiO_2 thin film. For a comparative study, we have obtained different magnetic parameters, *viz.*, the saturation magnetization (Ms) and coercivity (Hc) values from the *M-H* hysteresis curve of r-GO, TiO_2, and r-GO/TiO_2 show that the (Ms) and coercivity (Hc) have higher values in r-GO/TiO_2.

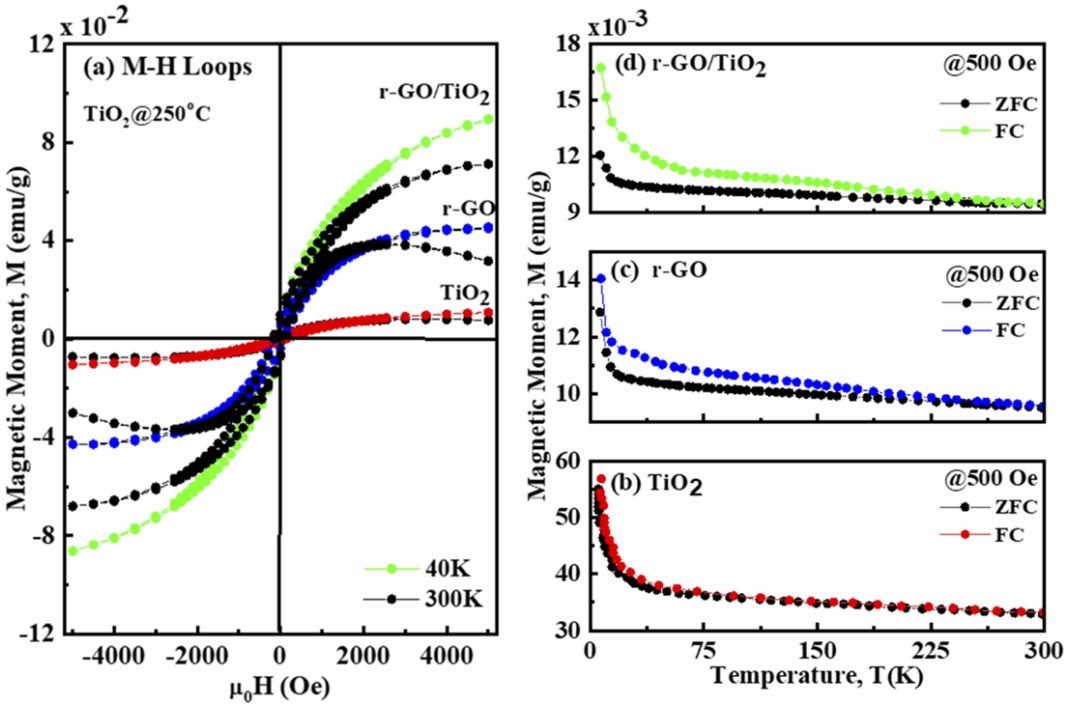

Figure 15. (a) M-H hysteresis loops and (b)–(d) M-T curve of r-GO, TiO_2, and r-GO/TiO_2 composites [153].

These enhanced magnetic performances of r-GO/TiO_2 comes from the vacancies/defects that induce magnetic moment at the interface of TiO_2 and r-GO. The ferromagnetism in the r-GO/TiO_2 composites is associated with various structural defects (O-/Ti-vacancies and O-/Ti-interstitials) present in the interface–lattice sites that induce magnetic moments. We believe that the magnetic performances are enhanced due to interactivity among magnetic Ti^{+}, O^{-}, and Ti-vacancies interstitial present at the interface of the r-GO/TiO_2 composite. It was attributed to the cutting of r-GO crystal during the oxidation/reduction process of various oxygen functional groups (–OH, –O–, –COOH, and C=O) that break the π bond network at grain boundaries [153] that induce magnetic domain. Figure 15b–d show the dependence of magnetic susceptibility on temperature for a composite r-GO/TiO_2 in the ZFC and FC modes at an applied magnetic field H = 500 Oe. There is a small difference in magnetic susceptibility in TiO_2 and r-GO/TiO_2 due to the possibility of setting some anti-parallel magnetic moments.

3.6.5. Ferromagnetic behavior of graphene oxide (GO) and molybdenum disulphide (MoS_2)-nanoparticles hybrid nanocomposite (GO:MoS_2-NPs)

In this work, Sarma et al. [154] has been made to explore the magnetic behaviours of GO, MoS_2-NP and GO:MoS_2-NP hybrid nanocomposites. GO:MoS_2-NP hybrid nanocomposites exhibit low temperature (at 45 K) ferromagnetism (LT-FM) after MoS_2-NP (diamagnetic) forming a hybrid nanocomposite with GO. Sarma et al. [154] also studied the divergence of field cooling (FC) and zero field cooling (ZFC) behaviours of GO:MoS_2-NP hybrid nanocomposite and forecast to be useful for low temperature magneticities, nuclear orientation and efficient flywheels for energy storage device application. For the low temperature magnetic application of these hybrid nanocomposites, M-H hysteresis loops for GO, MoS_2-NP and GO:MoS_2-NP were measured from -10 kOe < H < 10 kOe at low temperature at 45 K shown in Figure 16a and the field cooling (FC) and zero-field cooling (ZFC) of GO:MoS_2-NP hybrid nanocomposites is shown in Figure 16b. It is very interesting that the partial self-reversed magnetic hysteresis (SRMH) characteristics is observed in GO:MoS_2-NP hybrid nanocomposites after making a hybrid nanocomposite GO with MoS_2-NP [154–158]. The low temperature at 45 K magnetic hysteresis loops are shown in Figure 16a, where the magnetic saturation in MoS_2-NP and GO:MoS_2-NP hybrid nanocomposite is opposite to each other that confirms the SRMH effect of GO:MoS_2-NP hybrid nanocomposites [159]. The MoS_2-NP with Mo ~ 36%, S ~ 64% and have no C-content exhibits diamagnetic features, whereas GO:MoS_2-NP hybrid nanocomposite with C ~ 50%, O ~ 20%, Mo ~ 12%, S ~ 18% exhibit ferromagnetic nature.

Figure 16a shows that the M-H loops of MoS_2-NP exhibits diamagnetic behaviour unlike GO and GO: MoS_2-NP that exhibits LT-FM behaviour. Different magnetic parameters are obtained from Figure 3a and found that the saturation magnetization (M_S), coercivity (H_C) and remnant magnetization (M_R) of GO:MoS_2-NP nanocomposite are 5–10 times higher than GO. All magnetic parameters *viz*. M_S, H_C, M_R of GO and GO:MoS_2-NP hybrid nanocomposites are obtained and tabulated in Table 1. The saturation magnetization (M_S), coercivity (H_C) and remnant magnetization (M_R) of GO:MoS_2-NP nanocomposite are 3.6×10^{-3} emu/g, 2.5×10^{-3} emu/g and 1645 Oe, respectively. The GO:MoS_2-NP hybrid nanocomposites shows high coercivity (Hc) implying hard magnetic materials [160] and have SRHM behavior. The higher ferromagnetic behaviour shown in GO:MoS_2-NP hybrid nanocomposite is due to composite with GO. On adding of GO with MoS_2-NP different bonding *viz* C=C, C–OH, O–H/O–C–O, O–H, C–O and C–O radicals are attached with the

MoS_2-NPs that are responsible for ferromagnetic behaviours. The field cooling (FC), zero-field cooling (ZFC), temperature (T) and dependent magnetization (M) of the GO:MoS_2-NP hybrid nanocomposite is shown in Figure 16b. Sarma et al. [154] observed divergence in the FC curve and ZFC curve at T < 280 T and on increasing the magnetic field the divergence gradually disappears at ~280 K [161]. The disappearance of divergence with increased magnetic field is generally seen in magnetically frustrated systems, where usually ferromagnetic and antiferromagnetic bonds are randomly distributed. These behaviours are generally observed on few-layer 2D-graphene materials [162,163]. The appearance of ferromagnetic and SRMH behaviour in GO:MoS_2-NP hybrid nanocomposites could be very useful in low temperature magneticities, nuclear orientation and efficient flywheels for energy storage device application.

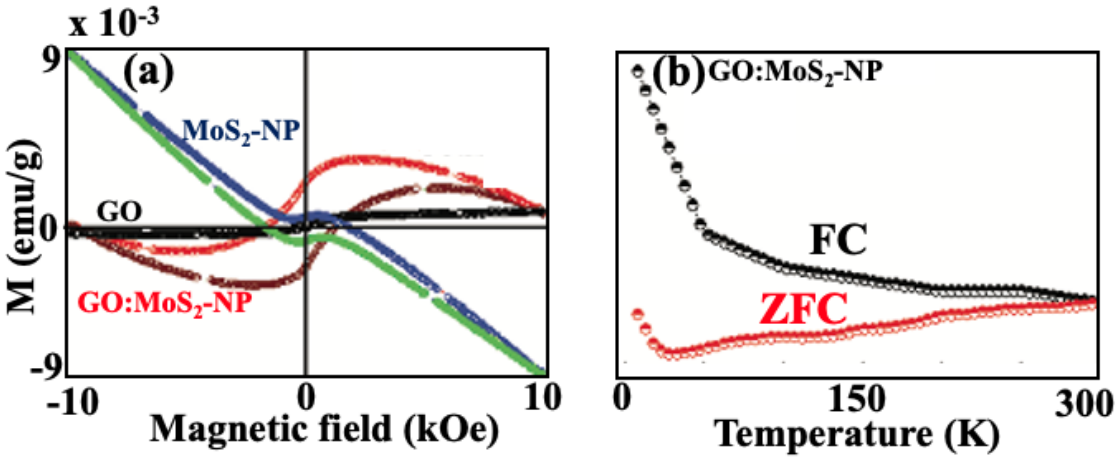

Figure 16. (a) Magnetisation (M) versus applied magnetic field ($\mu_0 H$) hysteresis loop of GO (black), MoS_2-NP (blue-forward and green- reverse) and GO:MoS_2-NP hybrid nanocomposite (red-reverse and wine-forward). (b) Zero field cooling (ZFC) and field cooling (FC) magnetization (M)-temperature (T) curve of GO:MoS_2-NP hybrid nanocomposite [154].

3.6.6. Ferro-magnetism of GO and carbon nanotubes (CNTs) nanocomposites

Nuhafizah et al. [164] studied the magnetic behaviours of the simple mixing of GO and carbon nanotubes (CNTs), i.e. GO:CNTs nanocomposites. In this process, graphene oxide (GO) is synthesized via a simple electrochemical exfoliation of graphite in a surfactant-containing aqueous solution; whereas CNTs are synthesized from waste engine oil using thermal chemical vapour deposition. Nuhafizah et al. [164] found that the addition of magnetic-CNTs has successfully induced the ferromagnetism in the GO at the room temperature. In this GO:CNTs composite materials, the saturation magnetization and average coercivity are observed to be ~6.13 $\times 10^{-3}$ emu/g and ~345.12 Oe, respectively. The presence of defects in carbonaceous GO and CNTs materials can induce spin polarization that enhances the magnetic properties of the GO:CNTs nanocomposites. This study offers a low cost and simple method to induce magnetism in GO as compared to the common chemical modifications of GO.

3.6.7. Magnetic properties of r-GO:$La_{0.9}Bi_{0.1}FeO_3$ nanocomposites

El-Khawas et al. [165] studied the magnetic behavioural change for the r-GO:$La_{0.9}Bi_{0.1}FeO_3$ (LBFO) nanocomposites. The ortho ferrite $La_{0.9}Bi_{0.1}FeO_3$ (LBFO) was prepared by the sol-gel autoignition method using the metal nitrates, lanthanum nitrate ($La(NO_3)_3{\cdot}6H_2O$), bismuth nitrate ($Bi(NO_3)_3{\cdot}5H_2O$) and ($Fe(NO_3)_3{\cdot}9H_2O$) as starting materials; whereas graphene oxide was prepared from graphite powder by the modified Hummer's method. Afterwards, the composites of LBFO and r-GO were prepared at different weight ratios of GO.

To prepare the r-GO:LBFO-nanocomposites, LBFO and r-GO were mixed together in 50 mL distilled water and ultrasonic for 1 h and dried in 70 ℃ for 12 h. The composites were then grinded for 30 min and finally annealed at 400 ℃ for 2 h with a heating/cooling rate of 5 ℃/min. The field-dependent magnetization (M vs. H) measurements at room temperature of r-GO:LBFO nanocomposites at different wt% of LBFO are shown in Figure 17. Figure shows that the r-GO enhances the magnetization of r-GO:LBFO nanocomposites. This behaviour can be explained by two reasons: (i) graphene can induce structural distortion on perovskite ($LaFeO_3$) crystal structure. This distortion originated from the interaction of oxygen functional groups of r-GO with $LaFeO_3$ that makes distortion in metal oxide, lead to variation in physicochemical properties [166–168]; (ii) the surface anisotropy of orthoferrite LFBO nanoparticles has been changed with the introduction of r-GO [169–171]. The exchange interface between r-GO and LFBO leads to modulate the surface spin and magnetic exchange anisotropy which leads to a change in values of exchange bias and its direction, as a result changes the magnetization of the composites.

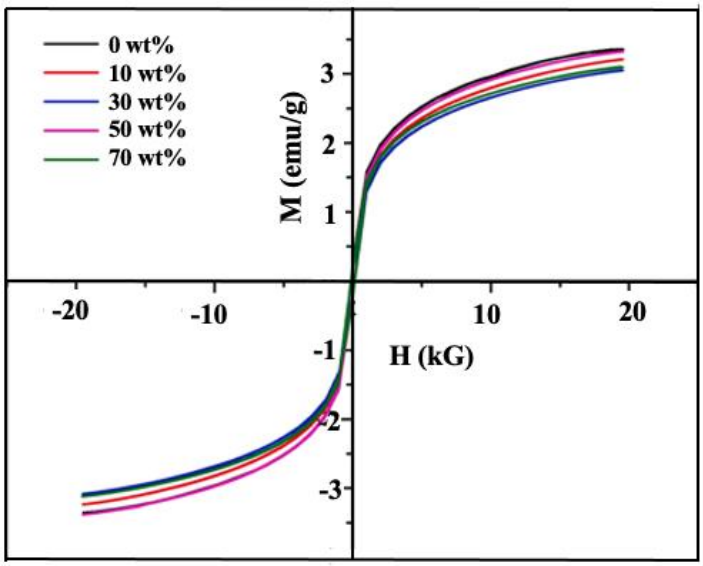

Figure 17. M-H hysteresis loops of rGO: LBFO nanocomposites at different LBFO wt% measured at room temperature (Reproduced from Ref. [165] with permission).

4. Discussion with brief theoretical perspective of magnetic performance in GO

As it is mentioned in the introduction section, the GO has a wrinkled layered with the combination of oxidized and non-oxidized regions those are randomly distributed. The oxidized

regions have -epoxide (C–O–C), hydroxyl (–OH), carbonyl (–C=O) and carboxyl (–COOH) that change the sp^2 carbon network completely. In the non-oxidized regions, the original sp^2 carbon network is preserved. In the oxidized regions, the epoxide and hydroxyl groups are bonded on both sides of the layer, where carbonyl (–C=O) and carboxyl (–COOH) occur at the edges of the layer. In reduction processes, the functional groups are partially removed and the sp^2 carbon network is partially restored. On reduction, GO is changed into reduced graphene oxide or simply r-GO. GO is electrically insulated due to the strong disruption of the sp^2 carbon network; whereas r-GO is a low conductor due to the partial restoration of the sp^2 network and have same types of defects occurring as in GO. The covalent functionalization of GO/r-GO induce magnetic moments. Interaction between randomly distributed magnetic moments in the single-layer GO/r-GO structural matrix is known as surface defects that produces antiferromagnetic ordering. The ferromagnetic ordering in zigzag graphene ribbons functionalized by an epoxy (C–O–C) pair-chain exhibits very charming electronic and magnetic properties. In the process of functionalization of any metal, non-metal, and/or (metal/non-metallic)-oxide, these are bonded with an oxygen functional radical and change the electronic structure and hence increase/decrease the magnetic performance on the whole. Furthermore, the sp^2, sp^3 and/or their ratio sp^2/sp^3 along with number of different oxygen functional groups modify the magnetism in GO/r-GO materials.

It has been observed and discussed that the magnetic behaviour of GO/r-GO in the limits of diamagnetism and ferromagnetism dependes on the degree of graphitization and the individual nature of the functional groups. In this context, the GO/r-GO preparation method plays a crucial role in controlling these functionalities, doping, intercalation, defects, formation of heterostructure, formation of nanocomposites and change of their density of states that decides the magnetism in GO. Whether induced magnetism appears in the GO/r-GO sheet depends on the fabrication process of the RGO sheet. If the reduction process of GO to r-GO left defects in the graphene sheet, then the induced magnetism may be significant. However, sometimes chemical modifications are not able to affect the magnetic properties of GO/r-GO sheets due to better reconstruction of the sp^2 bonding network. It is anticipated that clusters of defects that couple ferromagnetically behave like a single domain at low temperature, leading to the super-para magnetism. While at room temperature, other defects also effectively induce a magnetic moment, which gives rise to ferromagnetism but with a lower magnetic moment. The incorporation of atoms into GO results in substitutional impurities that forms ionic bonding between alkali metal adatoms and GO that have an adverse effect on the electronic states of the GO. On the other hand, group-III metals adatom showed mixed covalent bonding and ionic bonding that influence the lattice of GO a little bit. Nevertheless, 3d transition metal exhibits strong covalent bonding with GO layers. As a result of strong hybridization between the $d_{x^2-y^2}$ and d_{yz} orbitals of the 3d transition metal atoms and p_z orbitals of the carbon atoms, charge transfer takes place from the *d*-metal to the GO that are responsible for the magnetization in GO. In these low dimensional magnetic systems like GO, the surfaces, interfaces, thin-films, and porous structures, lowered symmetry and coordination number also offers a variety of structural change. The huge atomic heterogeneity of high-entropy materials along with a possibility to unravel the behaviour of individual components at the atomic scale suggests a great change of electronic structure that changes the magnetic performances of the GO/r-GO and/or r-GO-nanocomposites. The electronic structure modification in magnetic ordering of native/oxygen vacancy induced magnetization and the magnetic ordering is attributed to the asymmetric distribution of spin polarized

charge density in the vicinity of oxygen sites and/or sp^2/sp^3, which originates unequal from magnetic moment values. The change of band gaps and on-site electron correlation energy are also consequences on the magnetic properties of GO, r-GO and different oxide/sulphide-nanocomposites materials. The size and shape have also been crucial for tuning magnetic properties of GO. For instance, cutting of a GO sheet into two parts results in the formation of zigzag or armchair edges that alters the electronic properties of the GO sheets and hence magnetization.

In this structure, GO gets attracted towards the magnet forming the spin-like structure across the area of the magnet. The basic magnetic behaviour in GO is diamagnetism, but diverse magnetic properties are attributed to zigzag edges, defects, vacancies, adatoms, and various chemical functional-groups. It is discussed that the ferrimagnetism, para-magnetism in lower temperatures along with ferromagnetism and diamagnetism in higher temperatures exist in the multilayer graphene oxide. The transition of magnetic states of GO with changing temperature is discussed based on average anisotropy energy and coupling interactions. The wrinkled structure and the defects due to the surface functional groups play a significant role in shaping magnetism in GO. The zero-field cooling (ZFC)-field cooling (FC) curves also clarifies the picture of various phase transitions it is with change in temperature. The ZFC-FC curves are also analysed to explore the system further. With decreasing temperature, the magnetization increases reaching its highest value at <5 K. The GO/r-GO exhibit ferromagnetism due to the existence of various defects such as vacancy, topological defects or frustration, and the possible long-range ordered coupling among them. Defect-defect interaction depends on the vacancy location, ferromagnetic for vacancies in the same sublattices and antiferromagnetic for the different sublattices. The edge condition and surface functional groups or defects play a crucial role in terms of magnetic performances. The strong ferromagnetism is observed for GO flakes while the weak residual ferromagnetism of GO paper is due to magnetic moments surviving in the closed pores. The magnetization originated from the superimposition of a paramagnetic component, more pronounced at low temperatures, and a diamagnetic one, which was essentially temperature independent. At <5 K, the magnetization of both GO and r-GO was mainly determined by the paramagnetic signal, whereas at higher temperatures, the diamagnetic contribution became dominant, and the magnetization acquired negative values. The magnetization for both GO and r-GO was analysed using

$$M(H,T) = M_{PM} + M_{dia} = M_S B_S(x) + \chi_{dia} H,$$

Where M_{PM} describes the paramagnetic contribution with $M_0 = N_g S \mu_B$ being the saturation magnetization, g the effective g-factor, S the spin angular momentum, N the spin density, k_B the Boltzmann constant, and $B_S(x)$ the Brillouin function with $x = gS\mu_B H/k_B T$, while the second term $M_{dia} = \chi_{dia} H$ corresponds to a linear diamagnetic contribution with χ_{dia} (i.e. $\chi = M/H$) being the diamagnetic susceptibility. This behaviour was further explored by measuring the temperature dependence of the magnetization at constant magnetic field. In this case, a clear diamagnetic as well as paramagnetic contribution was evidenced at a specific temperature for GO and r-GO. This variation could be self-consistently described by the same expression as for the isothermal magnetization curves using the corresponding Brillouin function for $M(T)_H/H$ at constant magnetic field. This procedure could take into account the differences in M/H at different magnetic fields due to the nonlinear variation of $M(H)_T$. The magnetic susceptibilities of GO and r-GO could be well fitted by essentially the same parameters as for the $M(H)_T$ curves, verifying the interplay of diamagnetism/para-magnetism for the two systems. The corresponding ZFC-FC magnetization

shows 1/(M/H-χ_{dia}) *vs T* for GO and r-GO and the corresponding linear fits to the Curie law indicates the nature of magnetism. The ferromagnetism in GO/r-GO is intrinsic and their ferromagnetic susceptibility diminishes significantly with air. The magnetization of GO is decreased above >5 K. The ferromagnetism of GO/r-GO is correlated at zigzag edges. Transverse spin fluctuations accompanied by spin-flips of the magnetic moments of protons from hydroxyl groups cause the rapid decrease in magnetization >5 K. At higher temperatures, super-ferromagnetic and superparamagnetic states exist due to breaking of zig-zag edges of GO/r-GO.

4.1. Theoretical perspective of magnetic performance in GO

Graphene oxide (GO) is highly disordered and can exist as a monolayer or a few stacked layers having its basal planes decorated with OH (hydroxyl) and O (epoxy) groups, edges with COOH (carboxyl) and C=O (carbonyl) groups. It is insulating, unlike graphene which is highly conducting. Many theoretical works have predicted the possible reasons for the evolution of magnetism in graphene and graphene oxide. Unlike graphene where delocalized *p* electrons introduce diamagnetism, defects have the major decisive influence for the magnetism in GO. The sp^3 network [37,172] along with point defects (vacancies, adatom) [173], extended defects (zigzag edges, cracks, voids) [174,175] and topological defects (pentagons, heptagons and their combinations) [176] introduces localized magnetic moments in GO. In addition to this, the surface of GO carries ripples and corrugations, which also influence the magnetism [177,178]. The sp^3 network with the dangling bonds created by covalent functionalization of graphene acts as a source of magnetism in GO [37,116]. The pristine graphene is a half-filled bipartite system: the merger of two triangular sublattices A and B. Electrons of respective A and B sublattices correlate antiferromagnetically and the net magnetization (M) is proportional to (NA-NB) where NA and NB are the number of electrons in the two sublattices [96,179,180]. The GO is as a matrix of graphene decorated with oxygen functionalities. The epoxy (–O–), hydroxyl group (−OH) sits on the basal plane of GO and the carboxyl (−COOH), carbonyl (–C=O) groups prefer to acquire the edges of the GO sheets introducing new covalent bonds [181]. Different magnetic phases are seen at different temperature and field range. In the case of GO, the attachment of various mono and divalent functional groups on the surface leads to the formation of new bonds, defects and vacancies [181]. The charge transfer takes place between the functional groups and C atoms of graphene leading to electron imbalance between the two sublattices giving rise to a short-range anti-ferro-magnetism (ferrimagnetic) coupling around the defects and vacancies or the adsorbing site making it insulator or semi-metallic type [32,180]. In GO, loop opening takes place due to various anisotropy energies playing role on the surface of GO. Few of the attached OH groups assemble and forms clusters. These clusters coexist along with isolated OH groups on GO surface. The OH clusters carrying a bigger magnetic moment compared to isolated OH groups can act as non-interacting, randomly oriented single domain particles, responsible for irreversibility and opening of the hysteresis loop [180,181]. Theoretical investigations revealed that a major contribution to the ferromagnetism in GO comes from hydroxyl group (–OH) and –OH clusters. This random arrangement of –OH groups break the A, B lattice symmetry (bipartite system), giving rise to a localized state with uncompensated spin. Hence, a single –OH can produce a magnetic moment. If we think about an epoxy (–O–) group in which the oxygen bonds with an adjacent carbon atom at the edge, it preserves its symmetry and does not contribute to the total magnetic moment. But the epoxy (–O–) group bonds with a C–C bond that

breaks the C–C bond and forms ether (C–O–C) structure *zigzag* or *armchair*-edges. These *zigzag*-edges are important like defects because at the edge the electrons are energetically degenerate with highly localized states and unpaired spins giving rise to local magnetic moments at the edge boundaries. Again, GO consists of unreacted sp^2 regions along with reacted sp^3 regions. Partial distortion of layers results from oxygen groups in the reacted regions that are responsible for the magnetic moments. However, the shape, strain and surface anisotropy along with crystal anisotropy are expected to regulate the behaviour of M-H curves [57]. However, both the contributions of OH clusters and isolated OH groups vary with temperature, so anisotropy energy varies from site to site. The OH groups along with positive carbon matrix brings in the dipolar contribution, which leads to shape anisotropy. The spherical clusters have no input towards shape anisotropy, as the demagnetizing energy is uniform in all directions whereas the non-spherical clusters contribute to shape anisotropy. The attached functional groups, dangling bonds put stress to the GO matrix, inducing strain anisotropy in terms of magnetostatic energy. The strain and shape anisotropies lead to the absence of directions of hard and easy magnetization. The surface of GO is more crumpled because of the mismatch of thermal expansion coefficient between oxidized and unoxidized islands [178,182,183]. The OH clusters and isolated OH groups behave like spin units (localized electrons) with an insulating background. The numbers of spin units on the sheet are large due to the more sp^3 network because of which the local anisotropy energies should be large, but the random orientation of spins cancel out the effect to some extent. There is always a balance between anisotropy and exchange force, which results in a canted ferrimagnetic spin network interacting to each other with a short-range super-exchange interaction in the low field region. As the field, the nanosized single domain OH clusters along with the isolated ones try to align parallel with the external magnetic field, thus interaction among them is almost negligible. It has been observed that the complex behaviour of functionalized of GO, results in the large numbers of defects, vacancies, functional groups and zigzag edges leading to para-magnetism at low temperature and high field. The OH clusters are responsible for non-saturation of the M(H) curve [174,175,184]. Magnetism and the mechanism of magnetic coupling in graphene and GO decorated with monovalent and divalent adsorbates were investigated by many researchers using first-principles calculations based on spin polarized density functional theory. Wang et al. [46] have been investigated the magnetic properties of GO using spin-polarized first-principles density functional theory calculations. A series of structures with an epoxy-pair chain at various positions on zigzag graphene nanoribbons is considered as a model. The results show that this kind of GO is ferromagnetic at the ground state, providing great promise in the field of spintronics. During the oxidation process, the epoxy-pair structure is more favourable (a lower energy of 2.71 eV) rather than the scenario where an extra epoxy group is situated far from the existing epoxy chain. It is also indicated that only an energy of 0.1 eV is required to form one epoxy pair or add an epoxy group to extend the epoxy chain on graphene. It has been found that there is a high energy barrier of 0.76 eV for the reaction of one epoxy pair to form one carbonyl pair, although the existence of one carbonyl pair is 0.45 eV lower than one epoxy pair. Moreover, the energy barrier to break two neighbouring epoxy pairs into two carbonyl pairs approaches 1.07 eV, indicating that the alignment of epoxy pairs on graphene could be a relatively stable state. In comparison with zigzag graphene nanoribbons of the same width, this GO is metallic, and its spin density distribution is modified by epoxy pairs at different locations, thus rendering some fundamental insights into graphene materials. In order to study the influence of the hydroxyl/carboxyl groups on the electronic properties and hence magnetic performance of GO,

Hernández Rosas et al. [185] have calculated the gap energies of several structures with and without of these radical groups in GO. Hernández Rosas et al. [185] optimized the geometries for the different modelled structures and after calculation, it was found that on removing the carboxyl group, the gap energy increases up to 1.134 eV, suggesting a semimetal-semiconductor transition; on the other hand, on releasing the hydroxyl groups form the surface of graphene oxide, it decreases even further (0.404 eV). It is worth noting that on removing the carboxyl group the magnitude of the dipolar moment decreases considerably, even below that calculated for formic acid, suggesting that the carboxyl group is responsible of the polarity of graphene oxide. The structure of graphene oxide becomes unstable when the carboxyl group (COOH) was interchanged by either acid formic (HCOOH) or acetic acid (CH_3COOH). Furthermore, those functional groups depart from the surface by 3.184 and 3.17 Å, respectively. The same effect was obtained when the oxygen atom of the epoxy group was removed from the 2D structure. Li et al. [186] analysed the effects of adsorption concentration and the electronegativity of the adsorbate species on the magnetic and electronic properties. In this case, monovalent chemisorption, the magnetic order originates from the instability of *p* electrons induced by the adsorption, opening a narrow energy gap and resulting in antiparallel spin directions on adjacent carbon atoms on the graphene sheet. The magnetic order is only possible for the separation between the adsorbing sites of less than 10 Å. On the contrary, divalent chemisorption causes long-range magnetic coupling that originates from the exchange interactions between localized nonbonding *p* electrons (spin-polarized) mediated by the conduction *p* electrons around the Fermi energy, similar to the *s*–*d* interaction in transition metals. Temperature dependent magnetization (Ms), Remanence (M_R) and coercivity (Hc) values of different GOs are tabulate in Table 1.

Table 1. Magnetic parameters of different forms of graphene-oxide.

Sr. No.	GO and/or r-GO	Temperature (K)	Saturation magnetization (M_S) (emu/g)	Remanence (M_R) (emu/g)	Coercivity (H_C) (Oe)	(Refs.)
1	Graphite-oxide	300	6×10^{-3}	-	-	[1]
	Graphite-oxide heated at 600 ℃	-	0.45×10^{-3}	-	-	
2	GO	300	3000	-	150	[59]
	M-rGO	300	paramagnetic	-	-	
	H-rGO	300	paramagnetic	-	-	
3	r-GO	300	38.8×10^{-2}	-	-	[73]
		40	1.10×10^{-2}	-	-	
	r-GO:Au(nc)$_{0.22}$	300	1.20×10^{-2}	-	-	
		40	1.50×10^{-2}	-	-	
	r-GO:Au(nc)$_{4.88}$	300	Paramagnetic	-	-	
		40	Paramagnetic	-	-	
	Au(nc) ≈ 1.7 nm	300	Ferromagnetic	-	-	
	Au(nc) ≈ 5.0 nm	300	Diamagnetic	-	-	

Continued on next page

Sr. No.	GO and/or r-GO	Temperature (K)	Saturation magnetization (M_S) (emu/g)	Remanence (M_R) (emu/g)	Coercivity (H_C) (Oe)	(Refs.)
4	Bulk-Fe	300	220	-	0.90	[80,81]
	r-GO:Fe/Fe_2O_3	300	0.68×10^{-3}	-	11.0	
		1.8	0.93×10^{-3}	-	-	
5	Bulk Ni	300	58.57	-	0.7	[91,92,88]
	r-GO:Ni(*nc*)	300	20.4	2.3	103	[88]
6	r-GO:Pt-Ni(*nc*)	300	Ferromagnetic in nature	-	-	
	r-GO:Bi(*nc*)	300	Ferromagnetic in nature	-	-	
	r-GO:Pt(*nc*)	300	Diamagnetic in nature	-	-	
7	r-GO	2	0.11	-	-	[63]
	r-GO:N	2	1.66	0.039	160	
8	GO	300	6.8×10^{-5}	-	38	[76]
	GO:$N_{1.30}$	300	5.3×10^{-3}	-	10	
	GO:$N_{0.65}$	300	4.9×10^{-4}	-	19	
9	"Pyrrolic-N" groups provide a net magnetic moment of ≈0.95 μ_B/N atom					[102–105,62,52]
	"Pyridinic-N bonded to oxygen" provide a net magnetic moment of ≈0.56 μ_B/N atom					
	"OH" with graphene provide a net magnetic moment of ≈0.60 μ_B/"OH" radical					
10	*GO-N_x* from the Precursor(s) $C_6H_{12}N_4$	300	57×10^{-4}	-	53	[77]
	CH_4N_2O	300	31×10^{-4}	-	31	
11	*GO*	2	4.6×10^{-3}	-	-	[109]
	r-GO	2	5.6×10^{-3}	-	-	
	P-GO	2	5.5×10^{-3}	8.6×10^{-6}	-	
	P-rGO	2	9.6×10^{-3}		12	
12	*GO*	2	4.5×10^{-3}	-	-	[125]
	r-GO	2	5.6×10^{-3}	6.2×10^{-6}	5	
	CP-GO	2	2.9×10^{-3}	-	-	
	CP-rGO	2	5.1×10^{-3}	-	-	
13	*Fe_2O_3*	300	58.70	-	-	[135]
	r-GO:Fe_2O	300	1.63 & 30.30	-	-	
14	Bulk-Fe_3O_4	300	92	-	-	[139]
	Fe_3O_4-GO	300	3.45	-	-	
	Fe_3O_4-rGO	300	3.92	-	-	

Continued on next page

Sr. No.	GO and/or r-GO	Temperature (K)	Saturation magnetization (M_S) (emu/g)	Remanence (M_R) (emu/g)	Coercivity (H_C) (Oe)	(Refs.)
15	ZnO-NR	300	2.73×10^{-3}	-	37.1	[146]
	ZnO-NR:r-GO		6.29×10^{-2}		55	
	ZnO-NR(*nc*Au)		5.47×10^{-3}		68.7	
	ZnO-NR(*nc*Au):r-GO					
16	GO	300	3.53	2.08	358	[152]
	ZnO		55.4	2.54	321	
	S-rGO:ZnO		40.6	5.38	476	
	1H-rGO		9.05	3.51	439	
	2H-rGO		15.05	5.20	563	
	1H-rGO:ZnO		28.9	7.76	768	
	2H-rGO:ZnO		19.9	6.52	893	
17	r-GO:TiO_2	300	6.5×10^{-2}	6×10^{-2}	170	[153]
		40	9.5×10^{-2}	8×10^{-2}	200	
18	GO:MoS_2-NPs	45	3.6×10^{-3}	2.5×10^{-3}	1645	[154]
19	GO:CNTs	300	6.13×10^{-3}	-	345.12	[164]

5. Conclusion

The magnetic properties of GO and different GO's nanocomposites have been reviewed. The variation of saturation magnetization of GO and its different nanocomposites are varied with the defect density, oxide coverage, hydroxyl/epoxy relation and sp^2 and sp^3 domains. The magnetic moment at saturation (M_S) decreases with increasing oxygen-coverage and decreasing defect density. Magnetic saturation decreases with decreasing sp^2/sp^3 ratio. This can be attributed to the desorption of oxygen-coverage by the thermal decomposition method that are used during synthesis process, which increases the defect density and decreases sp^3 domains. Therefore, an increase in defect density, driven by oxygen-coverage desorption results in magnetization enhancement. It is also suggested that the origin of this magnetism and the magnetic moments in GO originate from the unpaired spins on the carbon radicals, caused by the presence of epoxy groups, whereas the presence of hydroxyl bridges in graphene oxide enhances magnetization. Therefore, these results suggest that topographic defects, like the boundary defect clusters observed, could be formed at atomic scale mainly by graphene decorated with hydroxyl and epoxy bridges. These could pull carbon atoms out of the plane of the graphene locally (carbon out-of-plane defect) and therefore uncompensated spins in GO systems appear. This effect is a possible mechanism responsible for ferromagnetic order in GOs. The stable FM induced by the adsorption of –OH atoms on graphene systems, also suggest that GO could play an important role in the development of low-cost graphene and oxidized graphene-based technologies. The variation in magnetic behaviour and the origin of ferromagnetism in GO is also identified as the C $2p(\sigma^*)$-derived states that involve defects/vacancies rather than the C $2p(\pi^*)$ states that are bound with oxygen-containing and hydroxyl groups on GO sheets. These results suggest future possibilities of the magnetism approach of GO, r-GO along with their different nanocomposites in spintronics of advanced sensors and other different devices applications.

Acknowledgements

SCR. gratefully acknowledge the financial support received from the National Research Foundation (NRF), South Africa (Grant No. EQP13091742446)

Use of AI tools declaration

No, I have not used.

Conflict of Interest

Author declare no competing financial interests and have no conflict of interest.

References

1. Lee D, Seo J (2017) Magnetic frustration of graphite oxide. *Sci Rep* 7: 44690. https://doi.org/10.1038/srep44690
2. Novoselov KS, Geim AK, Morozov SV, et al. (2005) Two-dimensional gas of massless Dirac fermions in graphene. *Nature* 438: 197–200. https://doi.org/10.1038/nature04233
3. Ohta T, Bostwick A, Seyller T, et al. (2006) Controlling the electronic structure of bilayer graphene. *Science* 313: 951–954. https://www.science.org/doi/10.1126/science.1130681
4. Chen H, Müller MB, Gilmore KJ, et al. (2008) Mechanically strong, electrically conductive and biocompatible graphene paper. *Adv Mater* 20: 3557–3561. https://doi.org/10.1002/adma.200800757
5. Zhang Y, Tan Y-W, Stormer HL, et al. (2005) Experimental observation of the quantum hall effect and Berry's phase in graphene. *Nature* 438: 201–204. https://doi:10.1038/nature04235
6. Maher P, Dean CR, Young F, et al. (2013) Evidence for a spin phase transition at charge neutrality in bilayer graphene. *Nat Phys* 9: 154–158. https://doi:10.1038/nphys2528
7. Huang L, Wu B, Yu G, et al. (2011) Graphene: learning from carbon nanotubes. *J Mater Chem* 21: 919–929. https://doi:10.1039/c0jm02225j
8. Yola ML, Eren T, Atar N (2014) A novel and sensitive electrochemical DNA biosensor based on Fe@Au nanoparticles decorated graphene oxide. *Electrochim. Acta* 125: 38–47. http://dx.doi.org/10.1016/j.electacta.2014.01.074
9. Gupta VK, Atar N, Yola ML (2014) A novel magnetic Fe@Au core-shell nanoparticles anchored graphene oxide recyclable nano-catalyst for the reduction of nitrophenol compounds. *Water Res* 48: 210–217. http://dx.doi.org/10.1016/j.watres.2013.09.027
10. Yola ML, Gupta VK, Eren T, et al. (2014) A novel electro analytical nano-sensor based on graphene oxide/silver nanoparticles for simultaneous determination of quercetin and morin. *Electrochim Acta* 120: 204–211. http://dx.doi.org/10.1016/j.electacta.2013.12.086
11. Yola ML, Eren T, Atar N (2015) A sensitive molecular imprinted electrochemical sensor based on gold nanoparticles decorated graphene oxide: application to selective determination of tyrosine in milk. *Sensor Actuat B-Chem* 210: 149–157. https://doi.org/10.1016/j.snb.2014.12.098

12. Yola ML, Atar N, Eren T, et al. (2015) Sensitive and selective determination of aqueous triclosan based on gold nanoparticles on polyoxometalate/reduced graphene oxide nanohybrid. *RSC Adv* 5: 65953–65962. https://doi.org/10.1039/C5RA07443F
13. Yola ML, Atar N (2017) A review: molecularly imprinted electrochemical sensors for determination of biomolecules/drug. *Curr Anal. Chem* 13: 13–17. https://doi.org/10.2174/1573411012666160601141018
14. Yola ML, Eren T, Atar N, et al. (2016) Direct-methanol fuel cell based on functionalized graphene oxide with mono-metallic and bi-metallic nanoparticles: electrochemical performances of nanomaterials for methanol oxidation. *Electroanalysis* 28: 570–579. https://doi.org/10.1002/elan.201500381
15. El çin S, Yola ML, Eren T, et al. (2016) Highly selective and sensitive voltammetric sensor based on ruthenium nanoparticle anchored calix[4]amidocrown-5 functionalized reduced graphene oxide: simultaneous determination of quercetin, morin and rutin in grape wine. *Electroanalysis* 28: 611–619. https://doi.org/10.1002/elan.201500495
16. Yokuş ÖA, Kardaş F, Akyıldırım O, et al. (2016) Sensitive voltammetric sensor based on polyoxometalate/reduced graphene oxide nanomaterial: application to the simultaneous determination of l-tyrosine and l-tryptophan. *Sensor Actuat B-Chem* 233: 47–54. http://dx.doi.org/10.1016/j.snb.2016.04.050
17. Yola ML, Atar N (2016) Functionalized graphene quantum dots with bi-metallic nanoparticles composite: sensor application for simultaneous determination of ascorbic acid, dopamine, uric acid and tryptophan. *J Electrochem Soc* 163: B718–B725. https://dx.doi.org/10.1149/2.1191614jes
18. Yola ML, Atar N (2017) A highly efficient nanomaterial with molecular imprinting polymer: carbon nitride nanotubes decorated with graphene quantum dots for sensitive electrochemical determination of chlorpyrifos. *J Electrochem Soc* 164: B223–B229. https://dx.doi.org/10.1149/2.1411706jes
19. Hummers WS, Offeman RE (1958) Preparation of graphitic oxide. *J Am Chem Soc* 80: 1339. https://pubs.acs.org/sharingguidelines
20. Alam SN, Sharma N, Kumar L (2017) Synthesis of graphene oxide by modified Hummers method and its Thermal reduction to obtain reduced graphene oxide. *Graphene* 6: 1–18. https://doi.org/10.4236/graphene.2017.61001
21. Nyangiwe NN, Khenfouch M, Thema FT, et al. (2015) Free-green synthesis and dynamics of reduced graphene sheets via sun light irradiation. *Graphene* 4: 54–61. https://doi.org/10.4236/graphene.2015.43006
22. Park S, An J, Potts JR. et al. (2011) Hydrazine-reduction of graphite- and graphene oxide. *Carbon* 49: 3019–3023. https://doi:10.1016/j.carbon.2011.02.071
23. Shin H-J, Kim KK, Benayad A, et al. (2009) Efficient reduction of graphite oxide by sodium borohydride and its effect on electrical conductance. *Adv Funct Mater* 19: 1987–1992. https://doi:10.1002/adfm.200900167
24. Pei S, Zhao J, Du J, et al. (2010) Direct reduction of graphene oxide films into highly conductive and flexible graphene films by hydrohalic acids. *Carbon* 48: 4466–4474. https://doi:10.1016/j.carbon.2010.08.006
25. Kamat PV (1993) Photochemistry on nonreactive and reactive (semiconductor) surfaces. *Chem Rev* 93: 267–300. https://doi.org/10.1021/cr00017a013

26. Zhou M, Wang Y, Zhai Y, et al. (2009) Controlled synthesis of large-area and patterned electrochemically reduced graphene oxide films. *Chem Eur J* 15: 6116–6120. https://doi.org/10.1002/chem.200900596
27. Wang Z, Zhou X, Zhang J, et al. (2009) Direct electrochemical reduction of single-layer graphene oxide and subsequent functionalization with glucose oxidase. *J Phys Chem C* 113: 14071–14075. https://doi.org/10.1021/jp906348x
28. Wang H, Robinson JT, Li X, et al. (2009) Solvothermal reduction of chemically exfoliated graphene sheets. *J Am Chem Soc* 131: 9910-9911. https://doi.org/10.1021/ja904251p
29. Park S, Ruoff RS (2009) Chemical methods for the production of graphenes. *Nat Nanotechnol* 4: 217–224. https://doi.org/10.1038/nnano.2009.58
30. Kan E, Li Z, Yang J (2008) Magnetism in graphene system. *Nano* 3: 433–442. https://doi.org/10.1142/S1793292008001350
31. Yazyev OV (2010) Emergence of magnetism in graphene materials and nanostructures. *Rep Prog Phys* 73: 056501. https://doi.org/10.1088/0034-4885/73/5/056501
32. Yazyev OV, Helm L (2007) Defect-induced magnetism in graphene. *Phys Rev B* 75: 125408. https://doi.org/10.1103/PhysRevB.75.125408
33. Yazyev OV, Katsnelson MI (2012) Theory of magnetism in grapheme, Advanced functional materials, *Science and Technology of Atomic, Molecular, Condensed Matter & Biological Systems*, Elsevier, 4: 71–103. https://dx.doi.org/10.1016/B978-0-44-453681-5.00004-2
34. Yazyev OV, Katsnelson MI (2008) Magnetic correlations at graphene edges: Basis for novel spintronics devices. *Phys Rev Lett* 100: 047209. https://doi.org/10.1103/PhysRevLett.100.047209
35. Golor M, Wessel S, Schmidt MJ (2014) Quantum nature of edge magnetism in graphene. *Phys Rev Lett* 112: 46601. https://doi.org/10.1103/PhysRevLett.112.046601
36. Li W, Zhao M, Xia Y, et al. (2009) Covalent-adsorption induced magnetism in graphene *J Mater Chem* 48: 9274–9282. https://doi.org/10.1039/b908949g
37. Santos EJG, Ayuela A, Sánchez-Portal D (2012) Universal magnetic properties of sp^3-type defects in covalently functionalized graphene. *New J Phys* 14: 43022. https://doi.org/10.1088/1367-2630/14/4/043022
38. Tang T, Tang N, Zheng Y, et al. (2015) Robust magnetic moments on the basal plane of the graphene sheet effectively induced by OH groups. *Sci Rep* 5: 8448. https://doi.org/10.1038/srep08448
39. Bagani K, Bhattacharya A, Kaur J (2014) Anomalous behaviour of magnetic coercivity in graphene oxide and reduced graphene oxide. *J Appl Phys* 115: 023902. https://doi.org/10.1063/1.4861173
40. Tang T, Liu F, Liu Y, et al. (2014) Identifying the magnetic properties of graphene oxide. *Appl Phys Lett* 104: 123104. https://doi.org/10.1063/1.4869827
41. Lee D, Seo J, Zhu XI, et al. (2015) Magnetism in graphene oxide induced by epoxy groups. *Appl Phys Lett* 106: 172402. https://doi.org/10.1063/1.4919529
42. Sinha A, Ali A, Thakur AD (2021) Ferromagnetism in graphene oxide. *Mater Today Proceed* 46: 6230–6233. https://doi.org/10.1016/j.matpr.2020.04.771
43. Mei X, Ouyang J (2011) Ultra sonication-assisted ultrafast reduction of graphene oxide by zinc powder at room temperature. *Carbon* 49: 5389–5397. https://doi.org/10.1016/j.carbon.2011.08.019

44. Sun P, Wang K, Wei J, et al. (2014) Magnetic transitions in graphene derivatives. *Nano Res* 7: 1507–1518. https://doi.org/10.1007/s12274-014-0512-1
45. Saremi S (2007) RKKY in half-filled bipartite lattices: Graphene as an example. *Phys Rev B* 76: 184430. https://doi.org/10.1103/PhysRevB.76.184430
46. Wang M, Li CM (2010) Magnetism in graphene oxide. *New J Phys* 12: 083040. https://doi.org/10.1088/1367-2630/12/8/083040
47. Fujii S, Enoki T (2010) Cutting of oxidized graphene into nanosized pieces. *J Am Chem Soc* 132: 10034–10041. https//doi.org/10.1021/ja101265r
48. Boukhvalov DW (2010) Modelling of hydrogen and hydroxyl group migration on graphene. *Phys Chem Chem Phys* 12: 15367–15371. https://doi.org/10.1039/c0cp01009j
49. Ghaderi N, Peressi M (2010) First-principle study of hydroxyl functional groups on pristine, defected graphene, and graphene epoxide. *J Phys Chem C* 114: 21625–21630. https://doi.org/10.1021/jp108688m
50. Boukhvalov DW (2013) DFT modeling of the covalent functionalization of graphene: From ideal to realistic models. *RSC Adv* 3: 7150–7159. https://doi.org/10.1039/C3RA23372C
51. Santos EJG, Ayuela A, Sánchez-Portal D (2012) Universal magnetic properties of sp^3-type defects in covalently functionalized graphene. *New J Phys* 14: 043022. https://doi.org/10.1088/1367-2630/14/4/043022
52. Wang M, Huang W, Chan-Park MB (2011) Magnetism in oxidized graphene with hydroxyl groups. *Nanotechnology* 22: 105702. https://doi.org/10.1088/0957-4484/22/10/105702
53. Strzelczyk R, Augustyniak-Jabtokow MA, Fedaruk R, et al. (2022) Edge ferromagnetism of graphene oxide. *J Mag Mag Mater* 544: 168686. https://doi.org/10.1016/j.jmmm.2021.168686
54. Radovic LR, Bockrath B (2005) On the Chemical nature of Graphene edge: origin of stability and potential for magnetism in carbon materials. 127: 5917–5927. https://doi.org/10.1021/ja050124h
55. Ray SC, Soin N, Makgato T, et al. (2014) Graphene supported graphone/graphane bilayer nanostructure material for spintronics. *Sci Rep* 4: 3862. https://doi.org/10.1038/srep03862
56. Boukhvalov DW, Katsnelson MI (2011) *sp*-electron magnetic clusters with a large spin in graphene. *ACS Nano* 5: 2440–2446. https://doi.org/10.1021/nn103510c
57. Bagani K, Ray MK, Satpati B, et al. (2014) Contrasting magnetic properties of thermally and chemically reduced graphene oxide. *J Phys Chem C* 118: 13254–13259. https://doi.org/10.1021/jp503034d
58. Chuang CH, Wang Y-F, Shao Y-C, et al. (2014) The effect of thermal reduction on the photoluminescence and electronic structures of graphene oxides. *Sci Rep* 4: 4525. https://doi.org/10.1038/srep04525
59. Wang YF, Singh SB, Limaye MV, et al. (2015) Visualizing chemical states and defects induced magnetism of graphene oxide by spatially-resolved-X-ray microscopy and spectroscopy. *Sci Rep* 5: 15439. https://doi.org/10.1038/srep15439
60. Ferrari AC, Meyer JC, Scardaci V, et al. (2006) Raman spectrum of graphene and graphene layers. *Phys Rev Lett* 97: 187401. https://doi.org/10.1103/PhysRevLett.97.187401
61. Ferrari AC, Robertson J (2000) Interpretation of Raman spectra of disordered and amorphous carbon. *Phys Rev B* 61: 14095–14107. https://doi.org/10.1103/PhysRevB.61.14095
62. Wang YY, Ni Zh, Yu T, et al. (2008) Raman studies of monolayer graphene: The substrate effect. *J Phys Chem C* 112: 10637–10640. https://doi.org/10.1021/jp8008404

63. Liu Y, Tang N, Wan X, et al. (2013) Realization of ferromagnetic graphene oxide with high magnetization by doping graphene oxide with nitrogen. *Sci Rep* 3: 2566. https://doi.org/10.1038/srep02566
64. Zhou JG, Wang J, Sun CL, et al. (2011) Nano-scale chemical imaging of a single sheet of reduced graphene oxide. *J Mater Chem* 21: 14622–14630. https://doi.org/10.1039/c1jm11071c
65. Schniepp HC, Li JL, McAllister MJ, et al. (2006) Functionalized single graphene sheets derived from splitting graphite oxide. *J Phys Chem B* 110: 8535–8539. https://doi.org/10.1021/jp060936f
66. Shen X, Lin X, Yousefi N, et al. (2014) Wrinkling in graphene sheets and graphene oxide papers. *Carbon* 66: 84–92. https://doi.org/10.1016/j.carbon.2013.08.046
67. Hua W, Gao B, Li S, et al. (2010) X-ray absorption spectra of graphene from first-principles simulations. *Phys Rev B* 82: 155433. https://doi.org/PhysRevB.82.155433
68. Jeong HK, Noh H-J, Kim J-Y, et al. (2009) Comment on "Near-edge X-ray absorption fine-structure investigation of graphene". *Phys Rev Lett* 102: 099701. https://doi.org/http://dx.doi.org/10.1103/PhysRevLett.102.099701
69. Pacilé D , Papagno, Rodr ́guez AF, et al. (2008) Near-edge X-ray absorption fine-structure investigation of graphene. *Phys Rev Lett* 101: 066806. https://doi.org/10.1103/PhysRevLett.101.066806
70. Pacilé D, Papagno M, Rodr ́guez AF, et al. (2009) Comment on "Near-edge X-ray absorption fine-structure investigation of graphene". *Phys Rev Lett* 102: 099702. https://doi.org/10.1103/PhysRevLett.102.099702
71. Ganguly A, Sharma S, Papakonstantinou P, et al. (2011) Probing the thermal deoxygenation of graphene oxide using high- resolution *in situ* X-ray-based spectroscopies. *J Phys Chem C* 115: 17009–17019. https://doi.org/10.1021/jp203741y
72. Zhou SY, Girit ÇÖ, Scholl A, et al. (2009) Instability of two-dimensional graphene: Breaking sp^2 bonds with soft X rays. *Phys Rev B* 80: 121409. https://doi.org/10.1103/PhysRevB.80.121409
73. Idisi DO, Ali H, Oke JA, et al. (2019) Electronic, electrical and magnetic behaviours of reduced graphene-oxide functionalized with silica coated gold nanoparticles. *Appl Surf Sci* 483: 106–113. https://doi.org/10.1016/j.apsusc.2019.03.271
74. Mondal A, Saha A, Sinha A, et al. (2012) Tunable catalytic performance and selectivity of a nanoparticle-graphene composite through finely controlled nanoparticle loading. *Chem Asian J* 7: 2931–2936. https://doi.org/10.1002/asia.201200716
75. Suda M, Kameyama N, Ikegami A, et al. (2009) Size-reduction induced ferromagnetism and photomagnetic effects in azobenzene-thiol- passivated gold nanoparticles. *Polyhedron* 28: 1868–1874. https://doi.org/10.1016/j.poly.2008.10.021
76. Sarma S, Ray SC, Strydom AM (2017) Electronic and magnetic properties of nitrogen functionalized graphene-oxide. *Dia Rel Mater* 79: 1–6. https://doi.org/10.1016/j.diamond.2017.08.011
77. Ghosh B, Sarma S, Pontsho M, et al. (2018) Tuning of magnetic behaviour in nitrogenated graphene oxide functionalized with iron oxide. *Dia Rel Mater* 89: 35–42. https://doi.org/10.1016/j.diamond.2018.08.006

78. Bhattacharya G, Kandasamy G, Soin N, et al. (2017) Novel π-conjugated iron oxide/reduced graphene oxide nanocomposites for high performance electrochemical super- capacitors. *RSC Adv* 7: 327–335. https://doi.org/10.1039/C6RA25630A
79. Zhang X, Liu J, He B, et al. (2014) Magnetic-resonance-based electrical properties tomography: A review. *IEEE Rev Biomed Eng* 7: 87–96. https://doi.org/10.1109/rbme.2013.2297206
80. Carmeli I, Skakalova V, Naaman R, et al. (2002) Magnetization of chiral monolayers of polypeptide a possible source of magnetism in some biological membranes. *Angew Chemie Int Ed Engl* 41: 761–764. https://doi.org/10.1002/1521-3773(20020301)41:5%3C761::AID-ANIE761%3E3.0.CO;2-Z
81. Idisi DO, Oke JA, Sarma S, et al. (2019) Tuning of electronic and magnetic properties of multifunctional r-GO-ATA-Fe_2O_3-composites for magnetic resonance imaging (MRI) contrast agent. *J Appl Phys* 126: 035301. https://doi.org/10.1063/1.5099892
82. Ionov AN, Volkov MP, Nikolaeva MN, et al. (2021) The magnetism of a composite based on reduced graphene oxide and polystyrene. *Nanomaterials* 11: 403. https://doi.org/10.3390%2Fnano11020403
83. Cong CJ, Liao L, Liu QY, et al. (2006) Effects of temperature on the ferromagnetism of Mn-doped ZnO nanoparticles and Mn-related Raman vibration. *Nanotechnology* 17: 1520–1526. https://doi.org/10.1088/0957-4484/17/5/059
84. Abdelbasir S, Shalan AE (2019) Intriguing properties and applications of functional magnetic materials, In: Sahu D, *Functional Materials*, IntechOpen, https://doi.org/10.5772/intechopen.81386
85. Goncalves G, Marques PAAP, Granadeiro CM, et al. (2009) Surface modification of graphene nanosheets with gold nanoparticles: The role of oxygen moieties at graphene surface on gold nucleation and growth. *Chem Mater* 21: 4796–4802. https://doi.org/10.1021/cm901052s
86. Yazyev OV, Helm L (2007) Defect-induced magnetism in graphene. *Phys Rev B* 75: 125408. https://doi.org/10.1103/PhysRevB.75.125408
87. Bozorth RM (1978) *Ferromagnetism*, Wiley-IEEE Press.
88. Sahoo PK, Panigrahy B, Li D, et al. (2013) Magnetic behaviour of reduced graphene oxide/metal nanocomposites. *J Appl Phys* 113: 17B525. https://doi.org/10.1063/1.4799150
89. Aktürk OÜ, Tomak M (2009) Au_nPt_n clusters adsorbed on graphene studied by first-principles calculations. *Phys Rev B* 80: 85417. https://doi.org/10.1103/PhysRevB.80.085417
90. Krasheninnikov AV, Lehtinen PO, Foster AS, et al. (2009) Embedding transition-metal atoms in graphene: Structure, bonding, and magnetism. *Phys Rev Lett* 102: 126807. https://doi.org/10.1103/PhysRevLett.102.126807
91. Chikazumi S, Charap SH (1964) *Physics of Magnetism*, New York: John Wiley & Sons.
92. Danan H, Meyer JP (1968) New determinations of the saturation magnetization of nickel and iron. *J Appl Phys* 39: 669. https://doi.org/10.1063/1.2163571
93. Lin D, Nunes AC, Majkrzak CF, et al. (1995) Polarized neutron study of the magnetization density distribution within a $CoFe_2O_4$ colloidal particle II. *J Magn Magn Mater* 145: 343. https://doi.org/10.1016/0304-8853(94)01627-5
94. Lu AH, Salabas EL, Schüth F, et al. (2007) Magnetic nanoparticles: Synthesis, protection, functionalization, and application. *Angew Chem Int Ed* 46: 1222. https://doi.org/10.1002/anie.200602866

95. Sun XC, Dong, XL (2002) Magnetic properties and microstructure of carbon encapsulated Ni nanoparticles and pure Ni nanoparticles coated with NiO layer. *Mater Res Bull* 37: 991. https://doi.org/10.1016/S0025-5408(02)00702-X
96. Matte HSSR, Subrahmanyam KS, Rao CNR (2009) Novel magnetic properties of graphene: presence of both ferromagnetic and antiferromagnetic features and other aspects. *J Phys Chem C* 113: 9982. https://doi.org/10.1021/jp903397u
97. Dutta S, Lakshmi S, Pati SK (2008) Electron-electron interactions on the edge states of graphene: A many-body configuration interaction study. *Phys Rev B* 77: 073412. https://doi.org/10.1103/PhysRevB.77.073412
98. Chen Y, Peng D-L, Lin D, et al. (2007) Preparation and magnetic properties of nickel nanoparticles via the thermal decomposition of nickel organometallic precursor in alkylamines. *Nanotechnology* 18: 505703. https://doi.org/10.1088/0957-4484/18/50/505703
99. Yang X, Xia H, Qin X, et al. (2009) Correlation between the vacancy defects and ferromagnetism in graphite. *Carbon* 47: 1399–1406. https://doi.org/10.1016/j.carbon.2009.01.032
100. Novoselov KS, Geim AK, Morozov SV, et al. (2004) Electric field effect in atomically thin carbon films. *Science* 306: 666–669. https://doi.org/10.1126/science.1102896
101. Nigar S, Zhou Z, Wang H, et al. (2017) Modulating the electronic and magnetic properties of graphene. *RSC Adv* 7: 51546–51580. https://doi.org/10.1039/C7RA08917A
102. Błoński P , Tuček J , Sofer Z, et al. (2017) Doping with graphitic nitrogen triggers ferromagnetism in graphene. *J Am Chem Soc* 139: 3171–3180. https://doi.org/10.1021/jacs.6b12934
103. Miao Q, Wang L, Liu Z, et al. (2016) Magnetic properties of N-doped graphene with high curie temperature. *Sci Rep* 6: 21832. https://doi.org/10.1038/srep21832
104. Ito Y, Christodoulou C, Nardi MV, et al. (2015) Tuning the magnetic properties of carbon by nitrogen doping of its graphene domains. *J Am Chem Soc* 137: 7678–7685. https://doi.org/10.1021/ja512897m
105. Denis PA (2022) Heteroatom co-doped graphene: The importance of nitrogen. *ACS Omega* 7: 45935–45961. https://doi.org/10.1021/acsomega.2c06010
106. Sun P, Wang K, Wei J, et al. (2014) Magnetic transitions in graphene derivatives. *Nano Res* 7: 1507–1518. https://doi.org/10.1007/s12274-014-0512-1
107. Wu Y, Yu D, Feng Y, et al. (2021) Facilely synthesized N-doped graphene sheets and its ferromagnetic origin. *Chinese Chem Lett* 32: 3841–3846. https://doi.org/10.1016/j.cclet.2021.04.054
108. Talukdar N, Wang Y, Nunna BB, et al. (2021) Nitrogen-doped graphene nanomaterials for electrochemical catalysis/reactions: A review on chemical structures and stability. *Carbon* 185: 198–214. https://doi.org/10.1016/j.carbon.2021.09.025
109. Gayan ES, Soin N, Moloi SJ, et al. (2020) Polyacrylate grafted graphene oxide nanocomposites for biomedical applications. *J Appl Phys* 127: 054302. https://doi.org/10.1063/1.5135572
110. Sarkar AK, Bediako JK, Choi J-W, et al. (2019) Functionalized magnetic biopolymeric graphene oxide with outstanding performance in water purification. *NPG Asia Mater* 11: 4. https://doi.org/10.1038/s41427-018-0104-8

111. Viswanathan C, Senthilkumar V, Sriranjini R, et al. (2005) Effect of substrate temperature on the properties of vacuum evaporated indium selenide thin films. *Cryst Res Technol* 40: 658. https://doi.org/10.1002/crat.200410404
112. Eda G, Fanchini G, Chhowalla M (2008) Large-area ultrathin films of reduced graphene oxide as a transparent and flexible electronic material. *Nat Nanotechnol* 3: 270. https://doi.org/10.1038/nnano.2008.83
113. Vozmediano MAH , López-Sancho MP, Stauber T, et al. (2005) Local defects and ferromagnetism in graphene layers. *Phys Rev B* 72: 155121. https://doi.org/10.1103/PhysRevB.72.155121
114. Li G, Luican A, Lopes de Santos JMB, et al. (2010) Observation of Van Hove singularities in twisted graphene layers. *Nat Phys* 6: 109–113. https://doi.org/10.1038/NPHYS1463
115. Eng AYS, Poh HL, Šaněk F, et al. (2013) Searching for magnetism in hydrogenated graphene. *ACS Nano* 7: 5930–5939. https://doi.org/10.1021/nn4016289
116. Qin S, Guo X, Cao Y, et al. (2014) Strong ferromagnetism of reduced graphene oxide. *Carbon* 78: 559–565. https://doi.org/10.1016/j.carbon.2014.07.039
117. Taniguchi T, Yokoi H, Nagamine M, et al. (2014) Correlated optical and magnetic properties in photo-reduced graphene oxide. *J Phys Chem C* 118: 28258–28265. https://dx.doi.org/10.1021/jp509399x
118. Enayati M, Nemati A, Zarrabi A, et al. (2019) The role of oxygen defects in magnetic properties of gamma-irradiated reduced graphene oxide. *J Alloys Compd* 784: 134–148. https://doi.org/10.1016/j.jallcom.2018.12.363
119. Enayati M, Nemati A, Zarrabi A, et al. (2018) Reduced graphene oxide: An alternative for magnetic resonance imaging contrast agent. *Mater Lett* 233: 363–366. https://doi.org/10.1016/j.matlet.2018.09.044
120. He Z, Yang X, Xia H, et al. (2011) Enhancing the ferro-magnetization of graphite by successive $12C^+$ ion implantation steps. *Carbon* 49: 1931–1938. https://doi.org/10.1016/j.carbon.2011.01.018
121. Soin N, Ray SC, Sarma S, et al. (2017) Tuning the electronic and magnetic properties of nitrogen functionalized few-layered graphene nanoflakes. *J Phys Chem* C 121: 14073. https://doi.org/10.1021/acs.jpcc.7b01645
122. Chuang C-H, Ray SC, Mazumder D, et al. (2017) Chemical modification of graphene oxide by nitrogenation: An x-ray absorption and emission spectroscopy study. *Sci Rep* 7: 42235. https://doi.org/10.1038/srep42235
123. Zhang K-C, Li Y-F, Liu Y, et al. (2016) Density-functional study on the structural and magnetic properties of N-doped graphene oxide. *Carbon* 102: 39–50. https://doi.org/10.1016/j.carbon.2016.02.030
124. Araki H, Yoshino K (1992) Preparation, molecular structures and novel magnetic properties of organic ferromagnetic compounds by pyrolysis of triphenoxy-triazine and benzoguanamine. *J Phys Condens Matter* 4: L119–L123. https://doi.org/10.1088/0953-8984/4/8/003
125. Ganya ES, Moloi SJ, Ray SC, et al. (2020) Tuning the electronic and magnetic properties of PEDOT-PSS-coated graphene oxide nanocomposites for biomedical applications. *J Mater Res* 35: 2478–2490. https://doi.org/10.1557/jmr.2020.236

126. Ray SC, Bhunia SK, Saha A, et al. (2015) Graphene oxide (GO)/reduced-GO and their composite with conducting polymer nanostructure thin films for non-volatile memory device. *Microelectron Eng* 146: 48–52. https://doi.org/10.1016/j.mee.2015.04.001
127. Eluyemi MS, Eleruja MA, Adedeji AV, et al. (2016) Synthesis and characterization of graphene oxide and reduced graphene oxide thin films deposited by spray pyrolysis method. *Graphene* 5: 143–154. http://dx.doi.org/10.4236/graphene.2016.53012
128. Roy S, Soin N, Bajpai R, et al. (2011) Graphene oxide for electrochemical sensing applications. *J Mater Chem* 21: 14725–14731. https://doi.org/10.1039/C1JM12028J
129. Ganguly A, Sharma S, Papakonstantinou P, et al. (2011) Probing the thermal deoxygenation of graphene oxide using high-resolution in situ X-ray-based spectroscopies. *J Phys Chem C* 115:17009–17019. https://doi.org/10.1021/jp203741y
130. Roy S, Soin N, Bajpai R, et al. (2011) Graphene oxide for electrochemical sensing applications. *J Mater Chem* 21: 14725-14731. https://doi.org/10.1039/c1jm12028j
131. Chang Y-S, Chen F-K, Tsai D-C, et al. (2021) N-doped reduced graphene oxide for room-temperature NO gas sensors. *Sci Rep* 11: 20719. https://doi.org/10.1038%2Fs41598-021-99883-9
132. Singh K, Ohlan A, Saini P, et al. (2008) Poly(3,4-ethylenedioxythiophene)γ-Fe_2O_3 polymer composite–super paramagnetic behavior and variable range hopping 1D conduction mechanism–synthesis and characterization. *Polym Adv Technol* 19: 229–236. https://doi.org/10.1002/pat.1003
133. Geng D, Yang S, Zhang Y, et al. (2011) Nitrogen doping effects on the structure of graphene. *Appl Surf Sci* 257: 9193–9198. https://doi.org/10.1016/j.apsusc.2011.05.131
134. Elk K, Richter J, Christoph V (1979) Density of states and electrical conductivity of disordered alloys with strong electron correlation. *J Phys F Met Phys* 9: 307–316. https://doi.org/10.1088/0305-4608/9/2/019
135. See TP, Pandikumar A, Ngee LH, et al. (2014) Magnetically separable reduced graphene oxide/iron oxide nanocomposite materials for environmental remediation. *Catal Sci Technol* 4: 4396–4405. https://doi.org/10.1039/C4CY00806E
136. Ren LL, Huang S, Fan W, et al. (2011) One-step preparation of hierarchical superparamagnetic iron oxide/graphene composites via hydrothermal method. *Appl Surf Sci* 258: 1132–1138. https://doi.org/10.1016/j.apsusc.2011.09.049
137. Tanwar S, Mathur D (2020) Magnetite-graphene oxide nanocomposites: Facile synthesis and characterization of optical and magnetic property. *Mater Today Proc* 30: 17–22. https://doi.org/10.1016/j.matpr.2020.03.745
138. Sepioni M, Nair RR, Rablen S, et al. (2010) Limits on intrinsic magnetism in graphene. *Phys Rev Lett* 105: 207205. https://doi.org/10.1103/PhysRevLett.105.207205
139. Popplewell J, Sakhnini L (1995) The dependence of the physical and magnetic properties of magnetic fluids on particle size. *J Magn Mater* 149: 72–78. https://doi.org/10.1016/0304-8853(95)00341-X
140. Thapa B, Diaz-Diestra D, Badillo-Diaz D, et al. (2029) Controlling the transverse proton relaxivity of Magnetic graphene-oxide. *Sci Rep* 9: 5633. https://doi.org/10.1038/s41598-019-42093-1

141. Wang GS, Chen GY, Wei ZY, et al. (2013) Multifunctional Fe_3O_4/graphene oxide nanocomposites for magnetic resonance imaging and drug delivery. *Mater Chem Phys* 141: 997–1004. https://doi.org/10.1016/j.matchemphys.2013.06.054
142. Cong HP, He JJ, Lu Y, et al. (2010) Water-soluble magnetic-functionalized reduced graphene oxide sheets: situ synthesis and magnetic resonance imaging applications. *Small* 6: 169–171. https://doi.org/10.1002/smll.200901360
143. Zhou GM, Wang DW, Zhang LL, et al. (2010) Graphene-wrapped Fe_3O_4 anode material with improved reversible capacity and cyclic stability for lithium ion batteries. *Chem Mater* 22: 5306–5313. https://doi.org/10.1021/cm101532x
144. Zhang M, Lei DN, Yin XM, et al. (2010) Magnetite/graphene composites: microwave irradiation synthesis and enhanced cycling and rate performances for lithium ion batteries. *Mater Chem* 20: 5538–5543. https://doi.org/10.1039/C0JM00638F
145. Koo HY, Lee HJ, Go HA, et al. (2011) Graphene-based multifunctional iron oxide nanosheets with tuneable properties. *Eur J* 17: 1214–1219. https://doi.org/10.1002/chem.201002252
146. Ray SC, Pong WF (2022) Possible Ferro-electro-magnetic performance of "reduced graphene oxide" deposited on "ZnO-nanorod (NR) decorated with nanocrystalline (nc) Au particles". *AIP Adv* 12: 055008. https://doi.org/10.1063/5.0091852
147. Ghosh B, Benecha EM, Ray SC, et al. (2019) ZnO nanorods decorated with nanocrystalline (*nc*) Au Particles: Electronic structure and magnetic behaviours. *J Alloys Compd* 797: 74–82. https://doi.org/10.1016/j.jallcom.2019.05.062
148. Qin S, Sun P, Di Q, et al. (2015) Ferromagnetism of three-dimensional graphene framework. *RSC Adv* 5: 92899–92904. https://doi.org/10.1039/c5ra14377b
149. Sun Z, Yang X, Wang C, et al. (2014) Graphene activating room-temperature ferromagnetic exchange in cobalt-doped ZnO dilute magnetic semiconductor quantum dots. *ACS Nano* 8: 10589–10596. https://doi.org/10.1021/nn5040845
150. Liu W, Speranza G (2021) Tuning the oxygen content of reduced graphene oxide and effects on its properties. *ACS Omega* 6: 6195–6205. https://doi.org/10.1021/acsomega.0c05578
151. Chen J, Zhang W, Sun Y, et al. (2016) Creation of localized spins in graphene by ring-opening of epoxy derived hydroxyl. *Sci Rep* 6: 26862. https://doi.org/10.1038/srep26862
152. Thiyagarajan K, Muralidharan M, Sivakumar K (2018) Interfacial ferromagnetism in reduced graphene oxide-ZnO nanocomposites. *J Mater Sci-Mater El* 29: 7442–7452. https://doi.org/10.1007/s10854-018-8735-7
153. Ray SC, Mishra DK, Wang HT, et al. (2022) Effects of electronic structure and magnetic performance at the surface/interface of r-GO and TiO_2 in r-GO/TiO_2 composite thin films: X-ray absorption near-edge structure and x-ray photoelectron spectroscopy. *AIP Adv* 12: 075101. https://doi.org/10.1063/5.0096305
154. Sarma S, Ray SC (2021) Low Temperature ferromagnetic behavior of graphene oxide (GO) and molybdenum disulphide (MoS_2) hybrid nanocomposite. *J Nanosci Nanotech* 21: 3320–3324. https://doi.org/10.1166/jnn.2021.19286
155. Ma J, Chen K (2017) Modulated self-reversed magnetic hysteresis in iron oxides. *Sci Rep* 7: 42312. https://doi.org/10.1038/srep42312
156. Yoshikazu I, Yasuhiko S (1963) Order-disorder transformation and reverse the remnant magnetism in the $FeTiO_3$-Fe_2O_3 system. *J Phys Chem Solids* 24: 517–528. https://doi.org/10.1016/0022-3697(63)90147-1

157. Nord GL, Lawson CA (1992) Magnetic properties of ilmenite70–hematite30: Effect of transformation-induced twin boundaries. *J Geophys Res* 97: 10897–10910. https://doi.org/10.1029/91JB02259
158. Hoffman KA (1992) Self-reversal of thermoremanent magnetization in the ilmenite-hematite system: Order-disorder, symmetry and spin alignment. *J Geophys Res* 97: 10883–10895. https://doi.org/10.1029/91JB02846
159. Dunin-Borkowski RE, Kasama T, Harrison RJ (2015) Electron Holography of nanostructured materials, In: Kirkland AI, Haigh SJ, *Nanocharacterisation*, The Royal Society of Chemistry, 2Eds., 158–210. http://dx.doi.org/10.1039/9781782621867-00158
160. Ghosh B, Ray SC, Pattanaik S, et al. (2018) Tuning of electronic structure and magnetic properties of Xenon ion implanted zinc oxide. *J Phys D-Appl Phys* 51: 095304. https://doi.org/10.1088/1361-6463/aaa832
161. Matte HSSR, Maitra U, Kumar P, et al. (2012) Synthesis, characterization, and proper- ties of few-layer metal dichalcogenides and their nanocomposites with noble metal particles polyaniline, and reduced graphene oxide. *ZAAC* 638: 2617–2624. https://doi.org/10.1002/zaac.201200283
162. Matte HSSR, Subrahmanyam KS, Rao CNR (2009) Novel magnetic properties of graphene: Presence of both ferromagnetic and antiferromagnetic features and other aspects. *J Phys Chem C* 113:9982–9985. https://doi.org/10.1021/jp903397u
163. Rao CNR, Matte HSSR, Subrahmanyam KS, et al. (2012) Unusual magnetic properties of graphene and related materials. *Chem Sci* 3: 45–52. https://doi.org/10.1039/C1SC00726B
164. Nurhafizah MD (2020) Magnetic properties of graphene oxide vis a simple mixing with waste engine oil-based carbon nanotubes. *SN Appl Sci* 2: 534. https://doi.org/10.1007/s42452-020-2361-8
165. El-Khawas EH, Azab AA, Mansour AM (2020) Structural, magnetic and dielectric properties of reduced graphene oxide/$La_{0.9}Bi_{0.1}FeO_3$ nanocomposites. *Mater Chem Phys* 241: 122335. https://doi.org/10.1016/j.matchemphys.2019.122335
166. Tepel M, Nesbit O, Tokmak F, et al. (1998) Sodium-dependent Cl^-/HCO_3^- exchange in patients with chronic renal failure: correlation with renal function. *Kidney Int* 53: 432–438. https://doi.org/10.1046/j.1523-1755.1998.00776.x
167. Peña MA, Fierro JLG (2001) Chemical structures and performance of perovskite oxides. *Chem Rev* 101: 1981–2017. https://doi.org/10.1021/cr980129f
168. Xia Z, Poeppelmeier KR (2017) Chemistry-inspired adaptable framework structures. *Acc Chem Res* 50: 1222–1230. https://doi.org/10.1021/acs.accounts.7b00033
169. Li T, Shen J, Li N, et al. (2013) Hydrothermal preparation, characterization and enhanced properties of reduced graphene-$BiFeO_3$ nanocomposite. *Mater Lett* 91: 42–44. https://doi.org/10.1016/j.matlet.2012.09.045
170. Hu J, Wang L, Shi L, et al. (2014) Preparation of $La_{1-x}Ca_xMnO_3$ perovskite-graphene composites as oxygen reduction reaction electrocatalyst in alkaline medium. *J Power Sources* 269: 144–151. https://doi.org/10.1016/j.jpowsour.2014.07.004
171. Molina-García MA, Rees NV (2017) Dual-doped graphene/perovskite bifunctional catalysts and the oxygen reduction reaction. *Electrochem. Commun* 84: 65–70. https://doi.org/10.1016/j.elecom.2017.10.004

172. Dreyer DR, Park S, Bielawski CW and Ruoff RS (2010) The chemistry of graphite oxide. *Chem Soc Rev* 39: 228–240. https://doi.org/10.1039/B917103G
173. Nair RR, Sepioni M, Tsai IL, et al. (2012) Spin-half paramagnetism in graphene induced by point defects. *Nat Phys* 8: 199–202. https://www.nature.com/articles/nphys2183#Sec1
174. Bhowmick S, Shenoy VB (2008) Edge state magnetism of single layer graphene nanostructures. *J Chem Phys* 128: 244717. https://doi.org/10.1063/1.2943678
175. Chen L, Guo L, Li Z, et al. (2013) Towards intrinsic magnetism of graphene sheets with irregular zigzag edges. *Sci Rep* 3: 2599. https://doi.org/10.1038/srep02599
176. López-Sancho MP, De Juan F, Vozmediano MAH (2009) Magnetic moments in the presence of topological defects in graphene. *Phys Rev B-Condens Matter Mater Phys* 79: 075413. https://doi.org/10.1103/PhysRevB.79.075413
177. Krishnamoorthy K, Veerapandian M, Yun K, et al. (2013) The chemical and structural analysis of graphene oxide with different degrees of oxidation. *Carbon* 53: 38–49. https://doi.org/10.1016/j.carbon.2012.10.013
178. Thompson-Flagg RC, Moura MJB, Marder M (2009) Rippling of graphene. *Epl* 85: 46002. https://doi.org/10.1209/0295-5075/85/46002
179. Bagani K, Bhattacharya A, Kaur J, et al. (2014) Anomalous behaviour of magnetic coercivity in graphene oxide and reduced graphene oxide. *J Appl Phys* 115: 023902. https://doi.org/10.1063/1.4861173
180. Kumazaki H, Hirashima D (2008) Nonmagnetic-defect-induced magnetism in graphene. *Physica E* 40: 1703–1705. https://doi.org/10.1016/j.physe.2007.10.112
181. Li W, Zhao M, Xia Y, et al. (2009) Covalent adsorption induced magnetism in graphene. *J Mater Chem* 19: 9274–9282. https://doi.org/10.1039/B908949G
182. Tang T, Liu F, Liu Y, et al. (2014) Identifying the magnetic properties of graphene oxide. *Appl Phys Lett* 104/12: 123104. https://doi.org/10.1063/1.4869827
183. Bedanta S, Kleemann W (2009) Topical review supermagnetism. *J Phys D-Appl Phys* 42: 013001. https://doi.org/10.1088/0022-3727/42/1/013001
184. Fujii S, Enoki T (2010) Cutting of oxidized graphene into nanosized pieces. *J Am Chem Soc* 132: 10034–10041. https://doi.org/10.1021/ja101265r
185. Hernández Rosas JJ, Ramírez Gutiérrez RE, Escobedo-Morales A, et al. (2011) First principles calculations of the electronic and chemical properties of graphene, graphane, and graphene oxide. *J Mol Model* 17: 1133–1139. https://doi.org/10.1007/s00894-010-0818-1
186. Li W, Zhao M, Xia Y, et al. (2009) Covalent-adsorption induced magnetism in graphene. *J Mater Chem* 19: 9274–9282. https://doi.org/10.1039/b908949g

AIMS Press